

Girsanov reweighting for path ensembles and Markov state models

L. Donati, C. Hartmann, and B. G. Keller

Citation: *The Journal of Chemical Physics* **146**, 244112 (2017); doi: 10.1063/1.4989474

View online: <http://dx.doi.org/10.1063/1.4989474>

View Table of Contents: <http://aip.scitation.org/toc/jcp/146/24>

Published by the [American Institute of Physics](#)



**COMPLETELY
REDESIGNED!**

**PHYSICS
TODAY**

Physics Today Buyer's Guide
Search with a purpose.

Girsanov reweighting for path ensembles and Markov state models

L. Donati,¹ C. Hartmann,² and B. G. Keller^{1,a)}

¹Department of Biology, Chemistry, Pharmacy, Freie Universität Berlin, Takustraße 3, D-14195 Berlin, Germany

²Institute of Mathematics, Brandenburgische Technische Universität Cottbus-Senftenberg, Konrad-Wachsmann-Allee 1, D-03046 Cottbus, Germany

(Received 8 March 2017; accepted 26 May 2017; published online 28 June 2017)

The sensitivity of molecular dynamics on changes in the potential energy function plays an important role in understanding the dynamics and function of complex molecules. We present a method to obtain path ensemble averages of a perturbed dynamics from a set of paths generated by a reference dynamics. It is based on the concept of path probability measure and the Girsanov theorem, a result from stochastic analysis to estimate a change of measure of a path ensemble. Since Markov state models (MSMs) of the molecular dynamics can be formulated as a combined phase-space and path ensemble average, the method can be extended to reweight MSMs by combining it with a reweighting of the Boltzmann distribution. We demonstrate how to efficiently implement the Girsanov reweighting in a molecular dynamics simulation program by calculating parts of the reweighting factor “on the fly” during the simulation, and we benchmark the method on test systems ranging from a two-dimensional diffusion process and an artificial many-body system to alanine dipeptide and valine dipeptide in implicit and explicit water. The method can be used to study the sensitivity of molecular dynamics on external perturbations as well as to reweight trajectories generated by enhanced sampling schemes to the original dynamics. *Published by AIP Publishing.* [<http://dx.doi.org/10.1063/1.4989474>]

I. INTRODUCTION

Molecular dynamics (MD) simulations with explicit solvent molecules are routinely used as efficient importance sampling algorithms for the Boltzmann distribution of molecular systems. From the conformational snapshots created by MD simulations, one can estimate phase-space ensemble averages and thus interpret experimental data or thermodynamic functions in terms of molecular conformations.

In recent years, the scope of MD simulations has considerably widened, and the method has been increasingly used to construct models of the conformational dynamics.^{1–5} Most notably Markov state models (MSMs),^{6–14} in which the conformational space is discretized into disjoint states and the dynamics is modeled as a Markov jump process between these states, have become a valuable tool for the analysis of complex molecular dynamics.^{15–19}

For the construction of dynamic models, one has to estimate path ensemble averages. For example, in MSMs, the transition probabilities between a pair of states B_i and B_j are estimated by considering a set of paths $S_\tau = \{\omega_1, \omega_2, \dots, \omega_n\}$, each of which has length τ , counting the number of paths which start in B_i and end in B_j and comparing this number to the total number of paths in the set (vertical line of blue boxes in Fig. 1).

Suppose, one would like to compare the dynamics in a reference potential energy function $V(\mathbf{r})$ to the dynamics in a series of perturbed potential energy functions $V(\mathbf{r}) + U(\mathbf{r}, \kappa)$, where $U(\mathbf{r}, \kappa)$ represents the perturbation and κ is a

tunable parameter, e.g., a force constant. While for phase-space ensemble averages, numerous methods exist to reweight the samples of the reference conformational ensemble to yield ensemble averages for the perturbed systems,^{20–23} similar reweighting schemes have not yet been developed for path ensemble averages of explicit-solvent simulations. This means that currently one would have to re-simulate the dynamics at each parameter value (vertical lines of green boxes in Fig. 1) and then construct a MSM for each simulation separately. This is computationally extremely costly.

An alternative would be to reweight the path ensemble average at the reference potential energy function to obtain path ensemble averages for the perturbed systems (reweighting box in Fig. 1). From measure theory, it is well known that a reweighting factor is given as the ratio between the probability measure associated with the reference potential energy function and the probability measure associated with the perturbed potential energy function. This applies to reweighting phase space ensemble averages as well as to reweighting path ensemble averages. Figure 2 illustrates the idea of a path ensemble reweighting method. The figure shows two sets of paths: one generated by a Brownian dynamics simulation without drift, S_τ [Fig. 2(a)], and the other generated by a Brownian dynamics simulation with drift, \tilde{S}_τ [Fig. 2(b)]. Both simulations sample the same path space $\Omega_{\tau,x}$ but the probability with which a given path is realized differs in the two simulations. In Figs. 2(a) and 2(b), the sets of paths, S_τ and \tilde{S}_τ , are colored according to their respective path probability density $\mu_P(\omega)$ and $\mu_{\tilde{P}}(\omega)$. Figures 2(c) and 2(d) show again S_τ ; this time however we colored the paths according to the probability density $\mu_{\tilde{P}}(\omega)$ with which they would have been generated by a

^{a)}Electronic mail: bettina.keller@fu-berlin.de

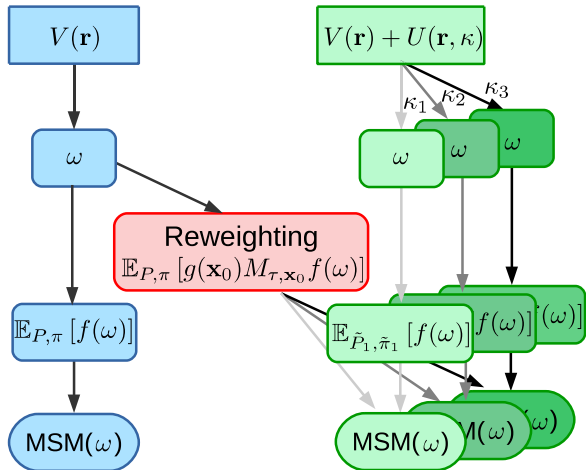


FIG. 1. Workflow of a reweighting scheme. $V(\mathbf{r})$ is the reference potential energy function, $V(\mathbf{r}) + U(\mathbf{r}, \kappa)$ is the perturbed potential energy function, where κ is a tunable parameter, ω is the trajectory generated by a MD simulation at the potential $V(\mathbf{r})$ or $V(\mathbf{r}) + U(\mathbf{r}, \kappa)$ and at a fixed thermodynamic state point. A MSM is an expected value with respect to a path probability measure P and a stationary distribution π , which can be estimated from the trajectory ω . A dynamical reweighting scheme, reweights the path probability measures P and π of the reference dynamics, to the path probability measures of a perturbed potential energy functions \tilde{P} and $\tilde{\pi}$. Thus, we can use the trajectory generated at $V(\mathbf{r})$ to estimate dynamical expected value (e.g., MSMs) at the perturbed potential energy functions.

Brownian dynamics with drift. For Brownian dynamics, this probability can be calculated directly [Fig. 2(c)]; for other types of dynamics, a reweighting method has to be used [Fig. 2(d)]. To estimate a path ensemble average for the Brownian dynamics with drift from S_T , the contribution of each path

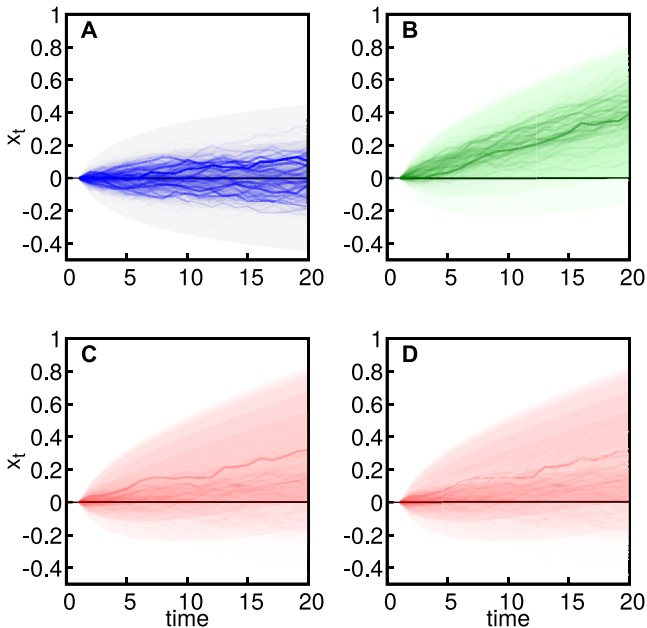


FIG. 2. Two sets of trajectories starting from $x(t=0)=0$ with time step $\Delta t=0.001$. (a) Set S_T generated by a Brownian motion without drift, associated with path probability measure P . Color intensity represents \tilde{P} . (b) Set S_T generated by a Brownian motion with drift $a=20$, associated with path probability measure \tilde{P} . (c) Set S_T , color intensity represents \tilde{P} (direct calculation). (d) Set S_T , color intensity represents \tilde{P} (Girsanov formula).

ω to the estimated value is multiplied by the ratio $M_{T,\mathbf{x}}(\omega) = \mu_{\tilde{P}}(\omega)/\mu_P(\omega)$ (Fig. 1).

Path ensemble reweighting schemes have initially been developed in the field of importance sampling for stochastic differential equations.^{24–26} For Langevin dynamics, the Girsanov theorem^{27,28} provides us with an expression for the probability ratio, and thus reweighting path ensemble averages become possible for this type of dynamics (Sec. II C). It has recently been demonstrated that the theorem can be applied to reweight Markov state models of Brownian dynamics in one- and two-dimensional potential energy functions.²⁹

Here we demonstrate how the Girsanov reweighting scheme can be applied to explicit-solvent all-atom MD simulations. For this, we need to address to critical pillars on which the Girsanov reweighting scheme rests:

- The equation of motion needs to contain a stochastic term which generates random forces drawn from a normal distribution (white noise).
- To calculate the reweighting factor, the random forces need to be accessible for each MD simulation step.

In all-atom MD simulations, the system is propagated by the Newton equations of motion which do not contain a stochastic term. We will discuss how the Girsanov theorem can nonetheless be applied to this type of simulation (Sec. IV B). The second point, in principle, requires that the forces are written out at every MD simulation step, i.e., at a frequency of femtoseconds rather than the usual output rate of several picoseconds. This quickly fills up any hard disc and slows the simulation by orders of magnitudes. We will present a computational efficient implementation of the reweighting scheme (Sec. IV A).

When applying the Girsanov theorem to reweight an MSM, an additional difficulty arises:

- The degrees of freedom which are affected by the perturbation might not be part of the relevant subspace of the MSM.

We found that the reweighting becomes problematic in this case and propose to project the perturbed degrees of freedom onto the relevant subspace during the estimation of the ratio of probability measures (Sec. II E).

The Girsanov reweighting method is demonstrated and benchmarked on several systems, ranging from two-dimensional diffusion processes (Sec. IV C), over molecular model systems which follow a Langevin dynamics (Sec. IV D), to all-atom MD simulations of alanine and valine dipeptides in explicit and implicit solvents (Sec. IV E).

II. THEORY

A. Molecular dynamics

Consider a molecular system with N particles, which evolves in time t according to the Langevin equation

$$M \frac{d\mathbf{v}(t)}{dt} = -\nabla V(\mathbf{r}(t)) - \gamma \mathbf{v}(t) + \sigma \eta(t),$$

$$\mathbf{v}(t) = \frac{d\mathbf{r}(t)}{dt}, \quad (1)$$

where M is the mass matrix and $\mathbf{r}(t)$ and $\mathbf{v}(t) \in \mathbb{R}^{3N}$ are the position vector and the velocity vector. $V(\mathbf{r})$ is the potential energy function. The interaction with the thermal bath is modelled by the friction coefficient γ , and an uncorrelated Gaussian white noise $\eta(t) \in \mathbb{R}^{3N}$ which is scaled by the volatility σ ,

$$\sigma = \sqrt{2k_B T \gamma M}, \quad (2)$$

where k_B is the Boltzmann constant and T is the temperature of the system.

The phase-space vector $\mathbf{x}(t) = \{\mathbf{r}(t), \mathbf{v}(t)\} \in \Gamma$ fully represents the state of the system at time t , where $\Gamma = \mathbb{R}^{6N}$ denotes the phase space of the system. The dynamics in Eq. (1) is associated with an equilibrium probability density

$$\mu_\pi(\mathbf{x}) = \frac{\exp[-\beta \mathcal{H}(\mathbf{x})]}{Z}, \quad (3)$$

where $\beta = \frac{1}{k_B T}$, $\mathcal{H}(\mathbf{x}) = \frac{1}{2} \mathbf{v}^\top M \mathbf{v} + V(\mathbf{r})$ is the classical Hamiltonian of the system, and $Z = \int_\Gamma \exp[-\beta \mathcal{H}(\mathbf{x})] d\mathbf{x}$ is the partition function. The function $\mu_\pi(\mathbf{x})$ is associated with the probability measure

$$\pi(A) = \mathbb{P}(\mathbf{x} \in A) = \int_A \mu_\pi(\mathbf{x}) d\mathbf{x}, \quad \forall A \subset \Gamma, \quad (4)$$

where $\pi(A)$ represents the equilibrium probability of finding the system in a subset A of the phase space Γ . The expected value of a function $a(\mathbf{x}) : \Gamma \rightarrow \mathbb{R}$ with respect to the probability density $\mu_\pi(\mathbf{x})$ is given as

$$\mathbb{E}_\pi[a] = \int_\Gamma a(\mathbf{x}) \mu_\pi(\mathbf{x}) d\mathbf{x} = \lim_{n \rightarrow \infty} \frac{1}{n} \sum_{\mathbf{x}_k \in S_n} a(\mathbf{x}_k), \quad (5)$$

where $S_n = \{\mathbf{x}_1, \dots, \mathbf{x}_n\}$ is a set of states distributed according to Eq. (3). When the phase space vectors \mathbf{x}_i are generated by numerically integrating Eq. (1), the second equality only holds if the sampling is ergodic. Equation (5) defines a *phase-space ensemble average*. The subscript π indicates the measure for which the expected value is calculated.

B. Path ensembles and MSMs

A path $\omega = \{\mathbf{x}(t=0) = \mathbf{x}_0, \mathbf{x}_1, \mathbf{x}_2, \dots, \mathbf{x}(\tau) = \mathbf{x}_n\}$ is a time-discretized realization of the dynamics $\mathbf{x}(t)$ on the time interval $[0, \tau = n \cdot \Delta t]$ starting at a particular point $\mathbf{x}_0 \in \Gamma$, where Δt is the time step and $n \in \mathbb{N}$ is the number of time steps. The associated path space is denoted as $\Omega_{\tau, \mathbf{x}} = \mathbb{R}^{6N \cdot n}$. A subset of the path space \mathcal{A} is constructed as a product of subsets $A_i \subset \Gamma$ of the state space $\mathcal{A} = A_1 \times A_2 \times \dots \times A_n$, where the subset A_i represents the phase space volume in which \mathbf{x}_i may be found. The probability that by integrating Eq. (1) one obtains a path ω which belongs to the subset $\mathcal{A} \subset \Omega_{\tau, \mathbf{x}}$ is given as

$$\begin{aligned} P(\mathcal{A}) &= \mathbb{P}(\omega \in \mathcal{A}) = \mathbb{P}(\mathbf{x}_1 \in A_1, \mathbf{x}_2 \in A_2, \dots, \mathbf{x}_\tau \in A_n) \\ &= \int_{A_1} \int_{A_2} \dots \int_{A_n} p(\mathbf{x}_0, \mathbf{x}_1; \Delta t) p(\mathbf{x}_1, \mathbf{x}_2; \Delta t) \dots p \\ &\quad \times (\mathbf{x}_{n-1}, \mathbf{x}_n; \Delta t) d\mathbf{x}_1 d\mathbf{x}_2 \dots d\mathbf{x}_n. \end{aligned} \quad (6)$$

The function $p(\mathbf{x}_i, \mathbf{x}_{i+1}; \Delta t)$ is the transition probability density, i.e., the conditional probability to be in \mathbf{x}_{i+1} after a time Δt given the initial state \mathbf{x}_i . The function P is a path probability measure and is the analogon to π in

phase space ensemble averages [Eq. (4)]. The path probability measure is associated with the path probability density function

$$\mu_P(\omega) = \mu_P(\mathbf{x}_1, \mathbf{x}_2, \dots, \mathbf{x}_\tau) = p(\mathbf{x}_0, \mathbf{x}_1; \Delta t) p(\mathbf{x}_1, \mathbf{x}_2; \Delta t) \dots p(\mathbf{x}_{n-1}, \mathbf{x}_n; \Delta t) \quad (7)$$

and hence the formal analogon to Eq. (4) in the path space is

$$P(\mathcal{A}) = \mathbb{P}(\omega \in \mathcal{A}) = \int_{\mathcal{A}} \mu_P(\omega) d\omega, \quad \forall \mathcal{A} \subset \Omega_{\tau, \mathbf{x}}, \quad (8)$$

where the integration over $d\omega$ is defined by Eq. (6).

Let $f : \Omega_{\tau, \mathbf{x}} \rightarrow \mathbb{R}$ be an integrable function, which assigns a real number to each path. The expected value of this function is

$$\begin{aligned} \mathbb{E}_P[f(\omega)] &= \int_{\Omega_{\tau, \mathbf{x}}} f(\omega) \mu_P(\omega) d\omega \\ &= \int_\Gamma \int_\Gamma \dots \int_\Gamma f(\mathbf{x}_1, \mathbf{x}_2, \dots, \mathbf{x}_n) \mu_P(\mathbf{x}_1, \mathbf{x}_2, \dots, \mathbf{x}_n) \\ &\quad \times d\mathbf{x}_1 d\mathbf{x}_2 \dots d\mathbf{x}_n \\ &= \lim_{m \rightarrow \infty} \frac{1}{m} \sum_{\omega_k \in S_{\tau, \mathbf{x}, m}} f(\omega_k), \end{aligned} \quad (9)$$

where we again assumed that the paths have a common initial state $\mathbf{x}(t=0) = \mathbf{x}_0$, and $S_{\tau, \mathbf{x}, m} = \{\omega_1, \omega_2, \dots, \omega_m\}$ corresponds to a set of paths of length τ generated by numerically integrating Eq. (1). When the paths are extracted from a single long trajectory, the last equality only holds if the sampling is ergodic. Equation (9) defines a *path ensemble average*. The subscript P indicates that the expected value is calculated with respect to a path probability measure.

For Markov processes, one can define a transition probability density $p(\mathbf{x}, \mathbf{y}; \tau)$, i.e., the conditional probability to be in $\mathbf{x}_n = \mathbf{y}$ after a time τ given that the path started in $\mathbf{x}_0 = \mathbf{x}$, by integrating the path probability density over all intervening states and applying recursively the Chapman-Kolmogorov equation

$$p(\mathbf{x}, \mathbf{y}, \tau) = \int_\Gamma \int_\Gamma \dots \int_\Gamma \mu_P(\mathbf{x}_1, \mathbf{x}_2, \dots, \mathbf{y}) d\mathbf{x}_1 d\mathbf{x}_2 \dots d\mathbf{x}_{n-1}. \quad (10)$$

Markov processes can be approximated by Markov state models.^{6-12,14} In these models, the phase space is discretized into disjoint sets (or microstates) B_1, B_2, \dots, B_s with $\cup_{i=1}^m B_i = \Gamma$, where the indicator function of the i th state is given as

$$\mathbf{1}_{B_i}(\mathbf{x}) := \begin{cases} 1, & \text{if } \mathbf{x} \in B_i, \\ 0, & \text{otherwise.} \end{cases} \quad (11)$$

The associated cross correlation function is

$$C_{ij}(\tau) = \int_\Gamma \mu_\pi(\mathbf{x}) \mathbf{1}_{B_i}(\mathbf{x}) \int_\Gamma p(\mathbf{x}, \mathbf{y}; \tau) \mathbf{1}_{B_j}(\mathbf{y}) d\mathbf{y} d\mathbf{x}, \quad (12)$$

where $\mu_\pi(\mathbf{x})$ is the equilibrium probability density [Eq. (3)]. The transition probability between set B_i and set B_j is

$$T_{ij}(\tau) = \frac{C_{ij}(\tau)}{\sum_{j=1}^s C_{ij}(\tau)}. \quad (13)$$

$T_{ij}(\tau)$ are the elements of the transition matrix whose dominant eigenvectors and eigenvalues represent the slow dynamic processes for the system.^{6-12,14}

Because of Eq. (10), one can regard the inner integral of the cross correlation function $C_{ij}(\tau)$ [Eq. (12)] as a path ensemble average [Eq. (9)] which depends on the initial state $\mathbf{x}_0 = \mathbf{x}$ of the path ensemble

$$\int_{\Gamma} p(\mathbf{x}, \mathbf{y}; \tau) \mathbf{1}_{B_j}(\mathbf{y}) d\mathbf{y} = \int_{\Gamma} \int_{\Gamma} \dots \int_{\Gamma} \mu_P(\mathbf{x}_1, \mathbf{x}_2, \dots, \mathbf{x}_n) \times \mathbf{1}_{B_j}(\mathbf{x}_n) d\mathbf{x}_1 d\mathbf{x}_2 \dots d\mathbf{x}_n = \mathbb{E}_P^{\mathbf{x}_0}[\mathbf{1}_{B_j}(\mathbf{x}_n)]. \quad (14)$$

This expected value is a linear operator and it is called the backward transfer operator. The outer integral in Eq. (12) is a phase space ensemble average, thus we have

$$\begin{aligned} C_{ij}(\tau) &= \int_{\Gamma} \mu_{\pi}(\mathbf{x}_0) \mathbf{1}_{B_i}(\mathbf{x}_0) \mathbb{E}_P^{\mathbf{x}_0}[\mathbf{1}_{B_j}(\mathbf{x}_n)] d\mathbf{x}_0 \\ &= \mathbb{E}_{\pi}[\mathbf{1}_{B_i}(\mathbf{x}_0) \mathbb{E}_P^{\mathbf{x}_0}[\mathbf{1}_{B_j}(\mathbf{x}_n)]] \\ &= \mathbb{E}_{P,\pi}[\mathbf{1}_{B_i}(\mathbf{x}_0) \mathbf{1}_{B_j}(\mathbf{x}_n)], \end{aligned} \quad (15)$$

where the combined phase space and ensemble average is defined as

$$\mathbb{E}_{P,\pi}[f(\omega)] = \int_{\Gamma} \mu_{\pi}(\mathbf{x}_0) \int_{\Omega_{\tau,\mathbf{x}}} f(\omega) \mu_P(\omega) d\omega d\mathbf{x}_0. \quad (16)$$

Equation (16) extends Eq. (9) to path ensembles with arbitrary initial states. The elements $C_{ij}(\tau)$ can be estimated from a set of paths of length τ , $S_{\tau,m} = \{\nu_1, \nu_2 \dots \nu_m\}$, in which the initial states are no longer fixed but are distributed according to $\mu_{\pi}(\mathbf{x})$,

$$\begin{aligned} C_{ij}(\tau) &= \lim_{m \rightarrow \infty} \frac{1}{m} \sum_{\nu_k \in S_{\tau}} \mathbf{1}_{B_i}([\nu_k]_{t=0}) \cdot \mathbf{1}_{B_j}([\nu_k]_{t=\tau}) \\ &= \lim_{m \rightarrow \infty} \frac{1}{m} \sum_{k=1}^m \mathbf{1}_{B_i}([\mathbf{x}_0]_k) \cdot \mathbf{1}_{B_j}([\mathbf{x}_n]_k), \end{aligned} \quad (17)$$

where $[\nu_k]_{t=i} = [\mathbf{x}_i]_k$ denotes the i th time step of the k th path.

C. Dynamical reweighting

We alter the reference dynamics [Eq. (1)] by adding a perturbation $U(\mathbf{r}) : \Gamma \rightarrow \mathbb{R}$ to the potential energy function $V(\mathbf{r})$. Thus, $\tilde{V}(\mathbf{r}) = V(\mathbf{r}) + U(\mathbf{r})$ is the perturbed potential energy function, and the Langevin equations of motion are

$$\begin{aligned} M \frac{d\mathbf{v}(t)}{dt} &= -\nabla \tilde{V}(\mathbf{r}(t)) - \gamma \mathbf{v}(t) + \sigma \eta(t), \\ \mathbf{v}(t) &= \frac{d\mathbf{r}(t)}{dt}. \end{aligned} \quad (18)$$

The perturbed dynamics is associated with a perturbed stationary probability density

$$\mu_{\tilde{\pi}}(\mathbf{x}) = \frac{\exp[-\beta \tilde{\mathcal{H}}(\mathbf{x})]}{\tilde{Z}}, \quad (19)$$

where $\tilde{\mathcal{H}}(\mathbf{x}) = \frac{1}{2} \mathbf{v}^T M \mathbf{v} + \tilde{V}(\mathbf{r})$ is the Hamiltonian of the perturbed system and \tilde{Z} is its partition function. The perturbation of the potential energy function also changes the transition probability density $\tilde{p}(\mathbf{x}_i, \mathbf{x}_{i+1}; \Delta t)$, which gives rise to a perturbed path probability density $\mu_{\tilde{p}}(\omega)$ [Eq. (7)] and a perturbed path measure \tilde{P} [Eq. (6)].

Reweighting methods compare the probability measure of the perturbed systems to the probability measure of a reference system. We first review the derivation of a reweighting

scheme for phase space probability measures before discussing path space probability measures. The perturbed phase-space probability measure $\tilde{\pi}$ is said to be *absolutely continuous* with respect to the reference phase space probability measure π if

$$\tilde{\pi}(A) = \int_A \mu_{\tilde{\pi}}(\mathbf{x}) d\mathbf{x} = 0 \Rightarrow \pi(A) = \int_A \mu_{\pi}(\mathbf{x}) d\mathbf{x} = 0. \quad (20)$$

This condition is sufficient and necessary to define the likelihood ratio between probability measures

$$g(\mathbf{x}) = \frac{d\tilde{\pi}}{d\pi} = \frac{\mu_{\tilde{\pi}}(\mathbf{x})}{\mu_{\pi}(\mathbf{x})} = \frac{Z}{\tilde{Z}} \exp(-\beta U(\mathbf{x})). \quad (21)$$

The function $g(\mathbf{x})$ is also called the Radon-Nikodym derivative (Radon-Nikodym theorem²⁸) and can be used to construct the phase-space probability measure of the perturbed system, from the phase-space probability of the reference system,

$$\tilde{\pi}(A) = \int_A \mu_{\tilde{\pi}}(\mathbf{x}) d\mathbf{x} = \int_A g(\mathbf{x}) \mu_{\pi}(\mathbf{x}) d\mathbf{x}. \quad (22)$$

As a consequence, if $g(\mathbf{x})$ can be calculated, one can estimate a phase space ensemble average [Eq. (5)] for the perturbed dynamics [Eq. (18)] from a set of states $S_n = \{\mathbf{x}_1, \dots, \mathbf{x}_n\}$ which has been generated by the reference dynamics [Eq. (1)]

$$\begin{aligned} \mathbb{E}_{\tilde{\pi}}[a] &= \int_{\Gamma} a(\mathbf{x}) \mu_{\tilde{\pi}}(\mathbf{x}) d\mathbf{x} = \int_{\Gamma} a(\mathbf{x}) g(\mathbf{x}) \mu_{\pi}(\mathbf{x}) d\mathbf{x} \\ &= \lim_{n \rightarrow \infty} \frac{1}{n} \sum_{k=1}^n a(\mathbf{x}_k) g(\mathbf{x}_k). \end{aligned} \quad (23)$$

The notion of absolute continuity is valid also for path probability densities,

$$\begin{aligned} \tilde{P}(A) = \int_A \mu_{\tilde{p}}(\omega) d\omega = 0 &\Rightarrow P(A) = \int_A \mu_P(\omega) d\omega = 0, \\ &\times \forall A \subset \Omega_{\tau,\mathbf{x}}. \end{aligned} \quad (24)$$

Thus we can reweight a path ensemble average, by using the likelihood ratio between the path probability density $\mu_{\tilde{p}}(\omega)$ and $\mu_P(\omega)$. For diffusion processes like (1) and (18), the likelihood ratio is given as

$$\begin{aligned} M_{\tau,\mathbf{x}}(\omega) = \frac{\mu_{\tilde{p}}(\omega)}{\mu_P(\omega)} &= \exp \left\{ \sum_{i=1}^{3N} \left[\sum_{k=0}^n \frac{\nabla_i U(\mathbf{r}_k)}{\sigma} \eta_k^i \sqrt{\Delta t} \right. \right. \\ &\quad \left. \left. - \frac{1}{2} \sum_{k=0}^n \left(\frac{\nabla_i U(\mathbf{r}_k)}{\sigma} \right)^2 \Delta t \right] \right\}, \end{aligned} \quad (25)$$

where η_k^i are the random numbers, along the dimension i at a time step k , generated to integrate Eq. (1) of the reference dynamics and $\nabla_i U(\mathbf{r}_k)$ is the gradient of the perturbation along the dimension i measured at the position \mathbf{r}_k . Note that to evaluate Eq. (25) one needs the positions and the random numbers for every time step of the time-discretized trajectory. Equation (25) is derived in Appendix B. We remark that the quantity $M_{\tau,\mathbf{x}}(\omega)$ exists also for continuous paths ($\Delta t \rightarrow 0$). In this case, the existence of the Radon-Nikodym derivative is guaranteed by the Girsanov theorem^{27,28} that states the conditions under which a perturbed path probability density \tilde{P} can be defined with respect to a reference path probability density P . The differences between time-continuous and time-discrete paths are discussed in Appendixes A and B.

Analogous to the reweighting of phase-space ensemble averages [Eq. (23)], we can use $M_{\tau,\mathbf{x}}(\omega)$ to reweight path ensemble averages

$$\begin{aligned}\mathbb{E}_{\tilde{P}}[f(\omega)] &= \int_{\Omega_{\tau,\mathbf{x}}} f(\omega) M_{\tau,\mathbf{x}}(\omega) \mu_P(\omega) d\omega \\ &= \lim_{n \rightarrow \infty} \frac{1}{n} \sum_{i=1}^n M_{\tau,\mathbf{x}}(\omega_i) f(\omega_i).\end{aligned}\quad (26)$$

The second equality shows how to estimate the path ensemble average $\mathbb{E}_{\tilde{P}}[f(\omega)]$ at the perturbed dynamics [Eq. (18)] from a set of paths $S_{\tau,\mathbf{x},m} = \{\omega_1, \omega_2, \dots, \omega_m\}$ which has been generated by the reference dynamics [Eq. (1)].

D. Reweighting MSMs

When reweighting a MSM, we estimate the cross correlation function $\tilde{C}_{ij}(\tau)$ for the perturbed dynamics [Eq. (18)], from a set of paths of length τ , $S_{\tau,m} = \{\nu_1, \nu_2 \dots \nu_m\}$, which has been generated by the reference dynamics [Eq. (1)]. The cross correlation function $\tilde{C}_{ij}(\tau)$ is a combined phase space and path ensemble average [Eq. (16)]. Thus, both averages have to be reweighted with the appropriated probability ratio,

$$\begin{aligned}\mathbb{E}_{\tilde{P},\tilde{\pi}}[a(\mathbf{x}_0)f(\omega)] &= \int_{\Gamma} a(\mathbf{x}_0) \mu_{\tilde{\pi}}(\mathbf{x}_0) \int_{\Omega_{\tau,\mathbf{x}}} f(\omega) \mu_{\tilde{P}}(\omega) d\omega d\mathbf{x}_0 \\ &= \int_{\Gamma} a(\mathbf{x}_0) g(\mathbf{x}_0) \mu_{\tilde{\pi}}(\mathbf{x}_0) \\ &\quad \times \int_{\Omega_{\tau,\mathbf{x}}} f(\omega) M_{\tau,\mathbf{x}}(\omega) \mu_P(\omega) d\omega d\mathbf{x}_0.\end{aligned}\quad (27)$$

With $a(\mathbf{x}_0) = \mathbf{1}_{B_i}(\mathbf{x}_0)$ and $f(\omega) = \mathbf{1}_{B_j}(\mathbf{x}_n)$, we obtain

$$\begin{aligned}\tilde{C}_{ij}(\tau) &= \mathbb{E}_{\tilde{P},\tilde{\pi}}[\mathbf{1}_{B_i}(\mathbf{x}_0) \mathbf{1}_{B_j}(\mathbf{x}_n)] \\ &= \int_{\Gamma} \mathbf{1}_{B_i}(\mathbf{x}_0) g(\mathbf{x}_0) \mu_{\tilde{\pi}}(\mathbf{x}_0) \\ &\quad \times \int_{\Omega_{\tau,\mathbf{x}}} \mathbf{1}_{B_j}(\mathbf{x}_n) M_{\tau,\mathbf{x}}(\omega) \mu_P(\omega) d\omega d\mathbf{x}_0,\end{aligned}\quad (28)$$

which can be estimated from a set of paths $S_{\tau,m} = \{\nu_1, \nu_2 \dots \nu_m\}$ as

$$\tilde{C}_{ij}(\tau) = \lim_{m \rightarrow \infty} \frac{1}{m} \sum_{\nu_k \in S_{\tau,m}} g([\mathbf{x}_0]_k) \mathbf{1}_{B_i}([\mathbf{x}_0]_k) \cdot M_{\mathbf{x},\tau}(\nu_k) \mathbf{1}_{B_j}([\mathbf{x}_n]_k),\quad (29)$$

where $[\mathbf{x}_i]_k$ is the i th time step of the k th path. As in Eq. (12), the initial states of the paths are not fixed but are distributed according to the equilibrium distribution $\mu_{\tilde{\pi}}(\mathbf{x})$ of the unperturbed dynamics. Finally, the transition probability between set B_i and set B_j for the perturbed dynamics is obtained as

$$\tilde{T}_{ij}(\tau) = \frac{\tilde{C}_{ij}(\tau)}{\sum_j \tilde{C}_{ij}(\tau)}.\quad (30)$$

The Radon-Nikodym derivative for path ensembles $g(\mathbf{x})$ contains the ratio of the partition functions Z/\bar{Z} as a multiplicative factor. Since this factor appears both in the numerator and the denominator of Eq. (30), it gets canceled, and the partition functions do not have to be calculated.

$T_{ij}(\tau)$ [and analogously $\tilde{T}_{ij}(\tau)$] is an element of the $s \times s$ MSM transition matrix $\mathbf{T}(\tau)$, where s is the number of disjoint sets (microstates). We characterize the MSM by plotting and analyzing the dominant left and right eigenvectors of the transition matrix

$$\begin{aligned}\mathbf{T}(\tau) \mathbf{r}_i &= \lambda_i(\tau) \mathbf{r}_i, \\ \mathbf{l}_i^T \mathbf{T}(\tau) &= \lambda_i(\tau) \mathbf{l}_i^T,\end{aligned}\quad (31)$$

where \mathbf{l}_i^T denotes the transpose of vector \mathbf{l}_i . We assess the approximation quality of the MSM by checking whether the implied time scales

$$t_i = -\frac{\tau}{\ln(\lambda_i(\tau))} = \text{const}, \quad \forall \tau > 0\quad (32)$$

are constant.^{9,12}

E. Projection

We now consider a perturbation $U(\cdot)$ that does not directly affect the relevant coordinates used to construct the MSM. In such a situation, the perturbation acts mainly on the coordinates directly perturbed and has a minor effect on the other degrees of freedom, in particular on the relevant coordinates that do not capture the full effect of the perturbation. Thus the reweighting may become problematic because the reweighting formula (25) is dominated by large, fluctuating gradients. To address this issue, we propose to project the gradient of the perturbation onto the coordinates used to construct the MSM. Let us assume that the MSM has been built on a combination of d coordinates χ_1, \dots, χ_d , then Eq. (25) is rewritten as

$$\begin{aligned}\hat{M}_{\tau,\mathbf{x}}(\omega) &= \frac{\hat{\mu}_{\tilde{P}}(\omega)}{\mu_P(\omega)} = \exp \left\{ \sum_{i=1}^{3N} \left[\sum_{k=0}^n \frac{\mathbf{c}_{i,k}}{\sigma_i} \eta_k^i \sqrt{\Delta t} \right. \right. \\ &\quad \left. \left. - \frac{1}{2} \sum_{k=0}^n \left(\frac{\mathbf{c}_{i,k}}{\sigma_i} \right)^2 \Delta t \right] \right\}\end{aligned}\quad (33)$$

with

$$\mathbf{c}_{i,k} = \sum_{j=1}^d \frac{\langle \nabla_i U(\mathbf{r}_k), \chi_{j,k} \rangle}{\langle \chi_{j,k}, \chi_{j,k} \rangle} \chi_{j,k}.\quad (34)$$

To understand why the projection reduces the variance of the estimator, note that $M = M_{\tau,\mathbf{x}}$ admits the decomposition $M = \hat{M}N$, where $\hat{M} = \hat{M}_{\tau,\mathbf{x}}$ denotes the part of the Radon-Nikodym derivative associated with the projected perturbation and $\hat{N} = \hat{N}_{\tau,\mathbf{x}}$ denotes the part corresponding to its orthogonal complement; for simplicity, we will drop the subscripts in the following. We call the relevant coordinates that enter \hat{M} the *resolved* coordinates and call all other coordinates *unresolved*.

Now let Z be any random variable that is independent of the unresolved variables. Then, for a fixed initial condition, the variance of the reweighted estimator is given by

$$\text{Var}[ZM] = \mathbb{E}_P[Z^2 M^2] - (\mathbb{E}_P[ZM])^2,\quad (35)$$

where $\mathbb{E}_P[Z^2 M^2] = \mathbb{E}_{\tilde{P}}[Z^2 M]$ and $\mathbb{E}_P[\cdot]$ denotes the expectation with respect to the reference measure P . Since the estimators with reweighting factor M or \hat{M} are both unbiased, it follows that the projection decreases the variance if

$$\mathbb{E}_{\tilde{P}}[Z^2 M] \geq \mathbb{E}_{\tilde{P}}[Z^2 \hat{M}].\quad (36)$$

TABLE I. Overview of the notation.

	State: \mathbf{x}	Path: ω
Space	$\Gamma \subset \mathbf{R}^{6N}$	$\Omega_{\tau, \mathbf{x}} = \Gamma^n \subset \mathbf{R}^{6N \cdot n}$
Subsets	$A_i \subset \Gamma$	$\mathcal{A} = \left(\prod_{i=1}^n A_i\right) \subset \Omega_{\tau, \mathbf{x}}$
Probability density	$\mu_{\pi}(\mathbf{x}) _{t \rightarrow \infty}$	$\mu_P(\omega)$
Probability of a state/path	$\pi(A) = \int_A \mu_{\pi}(\mathbf{x}) d\mathbf{x}$	$P(\mathcal{A}) = \int_{\mathcal{A}} \mu_P(\omega) d\omega$
Expected value	$\mathbb{E}_{\pi}[f(\mathbf{x})] = \int_A f(\mathbf{x}) \mu_{\pi}(\mathbf{x}) d\mathbf{x}$	$\mathbb{E}_P[f(\omega)] = \int_{\mathcal{A}} f(\omega) \mu_P(\omega) d\omega$
Absolute continuity	$\tilde{\pi}(A) = 0 \Rightarrow \pi(A) = 0$	$\tilde{P}(\mathcal{A}) = 0 \Rightarrow P(\mathcal{A}) = 0$
Radon-Nikodym derivative	$\frac{d\tilde{\pi}}{d\pi}$, see Eq. (21)	$\frac{d\tilde{P}}{dP}$, see Eq. (25)

In addition to Z being independent of the unresolved variables, we further assume that \hat{M} and N are independent under \tilde{P} , an assumption that is at least approximately satisfied in our case as is justified by the numerical experiments. As a consequence,

$$\mathbb{E}_{\tilde{P}}[Z^2 M] = \mathbb{E}_{\tilde{P}}[Z^2 \hat{M}] \mathbb{E}_{\tilde{P}}[N], \quad (37)$$

and it follows by Jensen's inequality and $N \geq 0$ that

$$1 = \mathbb{E}_{\tilde{P}}[1/N] \geq 1/\mathbb{E}_{\tilde{P}}[N], \quad (38)$$

which implies that $\mathbb{E}_{\tilde{P}}[N] \geq 1$. Note that $1 = \mathbb{E}_{\tilde{P}}[1/N]$ follows from the fact that $1/N$ is a probability density with respect to \tilde{P} . Further note that by the strict convexity of the function $f(x) = 1/x$ for $x \geq 0$, the inequality is strict unless N is \tilde{P} -a.s. constant. Hence, assuming that N is not constant, we conclude that (36) holds even strictly, which implies that elimination of the unresolved variables strictly decreases the variance of the estimator.

In Table I we summarize the main notation used in the theory section (Sec. II).

III. METHODS

A. Two-dimensional system

The Brownian dynamics on a two-dimensional potential energy function $V(x, y)$,

$$\begin{cases} dx_t = -\nabla_x V(x_t, y_t) + \sigma dB_t^x, \\ dy_t = -\nabla_y V(x_t, y_t) + \sigma dB_t^y, \end{cases} \quad (39)$$

has been solved using the Euler-Maruyama scheme³⁰ with an integration time step of $\Delta t = 0.001$. The term B_t^i denotes a standard Brownian motion in the direction $i = x, y$, $\sigma = 1$ is the volatility, and the random variables η^i were drawn from a standard Gaussian distribution. The reference potential energy function was

$$V(x, y) = (x^2 - 1)^2 + (y^2 - 1)^2 + |x - y|, \quad (40)$$

and the perturbed potential energy function was $\tilde{V}(x, y) = V(x, y) + U(y)$ with

$$U(y) = -y. \quad (41)$$

For both potential energy functions, trajectories of 8×10^7 time steps were produced. In both simulations, the path probability ratio $M_{\tau, \mathbf{x}}$ was calculated using Eq. (25). The MSMs have been constructed by discretizing each dimension x and y into 40 bins, yielding 1600 microstates. The chosen lag time was $\tau = 400$ time steps.

B. Many-body system in three-dimensional space

We designed a six-particle system, in which five particles form a chain while the sixth particle branches the chain at the central atom [Fig. 6(a)]. The position of the i th particle is $\mathbf{r}_i \in \mathbb{R}^3$. The potential energy between two directly bonded atoms [blue lines in Fig. 6(a)] was

$$V(\mathbf{r}_{ij}) = (\mathbf{r}_{ij}^2 - 1)^2 + 0.6\mathbf{r}_{ij} \quad (42)$$

with $\mathbf{r}_{ij} = \mathbf{r}_j - \mathbf{r}_i$. The bond potential energy function is a tilted double well potential. This ensures that the potential energy function of the complete system has multiple minima with varying depths. No non-bonded interactions were applied. Thus, the reference potential energy function of the complete system was

$$V(\mathbf{r}) = \sum_{ij=12,13,14,24,36} V(\mathbf{r}_{ij}). \quad (43)$$

The Langevin dynamics [Eq. (1)] of this system have been solved using the Brünger-Brooks-Karplus (BBK) integrator³¹ with an integration time step of $\Delta t = 0.001$. The masses M of the particles, the temperature T , the friction coefficient γ , and the Boltzmann constant k_B were all set to one. The perturbed potential energy function was $\tilde{V}(\mathbf{r}) = V(\mathbf{r}) + U(\mathbf{r})$ with

$$U(\mathbf{r}) = \frac{1}{2}\mathbf{r}_{24}^2 + \frac{1}{2}\mathbf{r}_{34}^2. \quad (44)$$

The perturbation is a harmonic potential energy along the through-space distance between atoms (2, 4) and (3, 4), respectively [green dashed line in Fig. 6(a)]. For both potential energy functions, trajectories of 3.2×10^8 time steps were produced. The MSMs were constructed on the two-dimensional space spanned by the bond-vectors \mathbf{r}_{12} and \mathbf{r}_{13} , i.e., on two coordinates which were not directly perturbed. Each dimension, x and y , has been discretized into 40 bins, yielding 1600 microstates. The chosen lag time was $\tau = 400$ time steps. In both simulations, the path probability ratio $M_{\tau, \mathbf{x}}$ was calculated by projecting the gradient vectors $\nabla U(\mathbf{r}_{24})$ and $\nabla U(\mathbf{r}_{34})$ on the vectors \mathbf{r}_{12} and \mathbf{r}_{13} and subsequently evaluating Eq. (33).

C. Alanine and valine dipeptides

We performed all-atom MD simulations of acetyl-alanine-methylamide (Ac-A-NHMe, alanine dipeptide) in implicit and explicit water and of acetyl-valine-methylamide (Ac-V-NHMe, valine dipeptide) in implicit water. All simulations

were carried out with the OPENMM 7.01 simulation package,³² in an NVT ensemble at 300 K. Each system was simulated with the force field AMBER ff-14sb.³³ The water model was chosen according to the simulation, i.e., the Generalized Born Surface Area (GBSA) model³⁴ for implicit solvent simulation and the TIP3P model³⁹ for explicit solvent simulation. For each of these setups, the aggregated simulation time was 1 μ s and we printed out the positions every `nstxout`=100 time steps, corresponding to 0.2 ps. A Langevin thermostat has been applied to control the temperature, and a Langevin leapfrog integrator³⁵ has been used to integrate Eq. (1). For implicit solvent simulations, interactions beyond 1 nm are truncated. For explicit solvent simulations, periodic boundary conditions are used with the Particle-Mesh Ewald (PME) algorithm³⁶ to estimate Coulomb interactions.

In the alanine dipeptide simulations, we have perturbed the potential energy function of the backbone dihedral angles ϕ and ψ . The reference potential energy functions

were

$$V(\phi) = 0.27 \cos(2\phi) + 0.42 \cos(3\phi), \quad (45)$$

$$V(\psi) = 0.45 \cos(\psi - \pi) + 1.58 \cos(2\psi - \pi) + 0.44 \cos(3\psi - \pi), \quad (46)$$

where the parameters have been extracted from force field files and π denotes the mathematical constant. The perturbed potential energy function was a harmonic potential along each dihedral angle degree of freedom,

$$U(\phi, \psi) = \frac{1}{2} \kappa_\phi \phi^2 + \frac{1}{2} \kappa_\psi \psi^2, \quad (47)$$

where κ_ϕ and κ_ψ are the force constants, which could be adjusted after the simulation [Figs. 7(a) and 7(b)]. The gradient $\nabla_{\mathbf{r}_i} U(\cdot)$ in Eq. (25) is defined with respect to the Cartesian coordinates. Thus, applying the chain rule, the path probability ratio for the perturbation of the backbone dihedral angles is given as

$$M_\tau = \exp \left\{ \sum_i^N \left[\kappa_\phi \int_0^\tau \frac{\phi(s)}{\sigma_i} \frac{\partial \phi(s)}{\partial \mathbf{r}_i} d\mathbf{B}_s^i + \kappa_\psi \int_0^\tau \frac{\psi(s)}{\sigma_i} \frac{\partial \psi(s)}{\partial \mathbf{r}_i} d\mathbf{B}_s^i - \frac{1}{2} \kappa_\phi^2 \int_0^\tau \left(\frac{\phi(s)}{\sigma_i} \frac{\partial \phi(s)}{\partial \mathbf{r}_i} \right)^2 ds - \frac{1}{2} \kappa_\psi^2 \int_0^\tau \left(\frac{\psi(s)}{\sigma_i} \frac{\partial \psi(s)}{\partial \mathbf{r}_i} \right)^2 ds + \kappa_\phi \kappa_\psi \int_0^\tau \frac{\phi(s)\psi(s)}{\sigma_i^2} \frac{\partial \phi(s)}{\partial \mathbf{r}_i} \frac{\partial \psi(s)}{\partial \mathbf{r}_i} ds \right] \right\}. \quad (48)$$

In the valine dipeptide simulation, we have perturbed the χ_1 side-chain dihedral angle. The reference potential energy function was

$$V(\chi) = 0.337 \cos(\chi) + 0.216 \cos(2\chi - \pi) + 0.001 \cos(4\chi - \pi) + 0.148 \cos(3\chi), \quad (49)$$

where the parameters have been extracted from force field files and π denotes the mathematical constant. The perturbed potential energy function was a harmonic potential,

$$U(\chi) = \frac{1}{2} \kappa_\chi \chi^2, \quad (50)$$

where κ_χ is the force constant, which could be adjusted after the simulation [Fig. 9(a)]. Thus, the path probability ratio is given as

$$M_\tau = \exp \left\{ \sum_i^N \left[\kappa_\chi \int_0^\tau \frac{\chi(s)}{\sigma_i} \frac{\partial \chi(s)}{\partial \mathbf{r}_i} d\mathbf{B}_s^i - \frac{1}{2} \kappa_\chi^2 \int_0^\tau \left(\frac{\chi(s)}{\sigma_i} \frac{\partial \chi(s)}{\partial \mathbf{r}_i} \right)^2 ds \right] \right\}. \quad (51)$$

The MSM, for both alanine dipeptide and valine dipeptide simulations, has been constructed by discretizing the dihedral angles ϕ and ψ into 36 bins each, yielding 1296 microstates. The chosen lag time was 20 ps for both the implicit and explicit solvent simulations.

To study the distribution of the force of the solvent on the solute, we have also performed one all-atom MD simulation of acetyl-alanine-methylamide in explicit water at 300 K, with the GROMACS 5.0.2 simulation package,³⁷ the force

field AMBER ff-99SB-ildn,³⁸ the TIP3P water model,³⁹ and the velocity-rescaling scheme.⁴⁰ The simulation time was 250 ns. We have printed out the trajectory and the total forces every 1 ps, and afterwards we have rerun the simulation, loading the saved trajectory but excluding the solvent. To obtain the value of the force of the solvent on the solute, we have subtracted the new forces to those initially saved.

IV. RESULTS AND DISCUSSION

A. Efficient implementation

To estimate a MSM at a perturbed potential energy function $V(\mathbf{x}) + U(\mathbf{x}, \kappa)$ with the dynamical reweighting method, one simulates a long trajectory $\mathbf{x}(t)$ at a reference potential energy function $V(\mathbf{x})$ using an integration time step Δt . From this trajectory m , short paths of length $\tau = n\Delta t$ are extracted, yielding a set of paths $S_{\tau,m} = \{v_1, v_2, \dots, v_m\}$, which can subsequently be used to evaluate Eq. (29), where $g([\mathbf{x}_0]_k)$ is given by Eq. (21) and $M_{\mathbf{x},\tau}(v_k)$ is given by Eq. (25) or Eq. (33). As discussed in Sec. II C, the factor Z/\bar{z} cancels for the estimate of $\tilde{T}_{ij}(\tau)$ [Eq. (30)] and the partition functions do not need to be calculated.

Let us assume that the simulation integrates the Langevin equations of motion for the reference potential energy function $V(\mathbf{x})$ [Eq. (1)]. To estimate a MSM with transition probabilities $\tilde{T}_{ij}(\tau)$ for the dynamics in the perturbed potential energy function from a set of paths $S_{\tau,m} = \{v_1, v_2, \dots, v_m\}$, we need to know the value of the perturbation $U([\mathbf{x}_i]_k, \kappa)$,

the gradient of the perturbation $\nabla U([\mathbf{x}_t]_k, \kappa)$ and the random numbers η_k generated at every time step of the simulation of each path v_k , and the volatility σ . The volatility is determined by the temperature and the friction coefficient [Eq. (2)], both of which are input parameters for the simulation algorithm.

In a naive implementation of the reweighting method, one would hence write out the positions and random numbers at every time step and calculate $g([\mathbf{x}_0]_k)$ and $M_{\mathbf{x},\tau}(v_k)$ in a post-analysis step. The advantage of this approach is that the set of paths can be reweighted to the path probability measure of any perturbation $U(\mathbf{x}, \kappa)$, as long as the absolute continuity is respected [Eq. (20)]. On the other hand, this approach is hardly practical because writing out a trajectory at every integration time step quickly fills up any hard disc and slows down the simulation considerably.

We therefore decided to compute the probability ratios $g([\mathbf{x}_0]_k)$ and $M_{\mathbf{x},\tau}(v_k)$ “on the fly” during the simulation. In practice, the lag time τ of a MSM can only assume values’ integer multiples of the frequency `nstxout` at which the positions are written to file, i.e., of $\tau = n\Delta t = A \cdot \text{nstxout} \cdot \Delta t$ with $A \in \mathbb{N}$. The discretized Itô integral and the discretized Riemann integral in Eq. (25) are sums from time step $k = 0$ to $k = n$, which can be broken down into A sums of size `nstxout`,

$$\sum_{k=0}^n \dots = \sum_{k=0}^{\text{nstxout}-1} \dots + \sum_{k=\text{nstxout}}^{2 \cdot \text{nstxout}-1} \dots + \dots + \sum_{k=(A-1) \cdot \text{nstxout}}^{A \cdot \text{nstxout}-1} \dots \quad (52)$$

Thus, we calculate the terms

$$I(a) = \sum_{i=1}^{3N} \sum_{k=(a-1) \cdot \text{nstxout}}^{a \cdot \text{nstxout}-1} \frac{\nabla_i U(\mathbf{r}_k)}{\sigma} \eta_k^i \sqrt{\Delta t} \quad (53)$$

and

$$R(a) = - \sum_{i=1}^{3N} \frac{1}{2} \sum_{k=(a-1) \cdot \text{nstxout}}^{a \cdot \text{nstxout}-1} \left(\frac{\nabla_i U(\mathbf{r}_k)}{\sigma} \right)^2 \Delta t \quad (54)$$

“on the fly” and write out the results at the same frequency `nstxout` as the positions. The path probability ratio is reconstructed after the simulation as

$$M_{\tau,\mathbf{x}}(\omega) = \exp \left\{ \sum_{a=1}^A I(a) + R(a) \right\}. \quad (55)$$

The potential energy of the perturbation $U(\mathbf{x}_t)$ is written out at the frequency `nstxout`, and the complete weight $g([\mathbf{x}_0]_k) \cdot M_{\mathbf{x},\tau}(v_k)$ is calculated during the construction of the MSM. The lag time τ can be chosen and varied after the simulation. The modification of the MD integrator can be readily implemented within the MD software package OpenMM.³² An example script is provided in the [supplementary material](#).

The approach requires that the perturbation potential energy function $U(\mathbf{r}, \kappa)$ is chosen prior to the simulation. Note however that if the perturbation potential energy function depends linearly on the parameter κ , i.e., if κ is a force constant $U(\mathbf{r}, \kappa) = \kappa \cdot U(\mathbf{r})$, then the two integrals are written as $I(a, U(\mathbf{r}, \kappa)) = \kappa \cdot I(a, U(\mathbf{r}))$ and $R(a, U(\mathbf{r}, \kappa)) = \kappa \cdot R(a, U(\mathbf{r}))$.

Thus, it is sufficient to calculate $I(a, U(\mathbf{r}))$ and $R(a, U(\mathbf{r}))$ “on the fly” and to scale the integrals after the simulation to any desired value of κ . A single simulation is sufficient to allow for reweighting a whole series of perturbation potential energy functions. Also, the integrator can be modified such that the Itô integrals $I_1(a), I_2(2) \dots$ and the Riemann integral $R_1(a), R_2(2) \dots$ of several functionally different perturbation energy functions $U_1(\mathbf{r}), U_2(\mathbf{r}) \dots$ are calculated. Thus, using a single reference simulation, one can reweight to several functionally different perturbations and scale these perturbations by an arbitrary force constant.

If the perturbation $U(\mathbf{r})$ affects only a small subset of all interactions in the system, the computational cost of calculating of $I_i(a)$ and $R_i(a)$ is modest. The blue line in Fig. 3 shows the computational costs for simulating alanine dipeptide in implicit water with $n = 0, 1, 2, 3, 4, 5$ different perturbations as the number of days required to obtain a trajectory of $1 \mu\text{s}$ for each perturbation on a small workstation. The red line in Fig. 3 shows the computational cost of implementing the same n perturbations into a single reference simulation. For a single perturbation, 30% of the computational cost is saved by dynamical reweighting, whereas for 5 perturbations more than half of the computational cost is saved. Note that the curve has been obtained by measuring the computational cost and not by extrapolating from the cost of a single perturbation. The gain is even greater, if the dependence on a force constant is to be studied. Moreover, in simulation boxes of larger systems with explicit solvent, the number of interactions affected by a typical perturbation is orders of magnitudes smaller than the total number of all interactions. Thus, the computational cost of calculating the integrals $I_i(a)$ and $R_i(a)$ “on the fly” becomes negligible. We remark that, if $I_i(a)$ and $R_i(a)$ are too large, the Girsanov reweighting method might become numerically intractable. This might be the case if the perturbation is too strong and hence $\nabla_i U(\mathbf{r})$ is large or if $\tau = n\Delta t$ is too large. Thus, a good discretization, which allows for the use of small lag times τ , is crucial in applying the Girsanov reweighting method to MSMs of larger molecules.

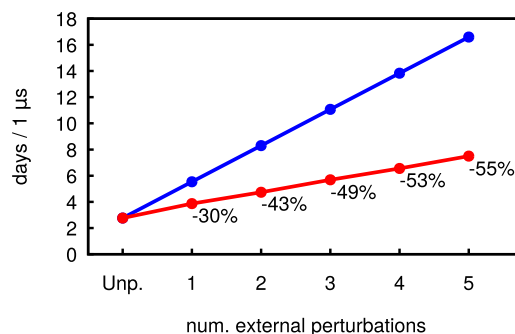


FIG. 3. Number of days needed to produce a trajectory of alanine dipeptide in implicit solvent of $1 \mu\text{s}$. The system has been perturbed by adding a harmonic potential to different dihedral angles. The blue line denotes the time needed to perform, respectively, 1, ..., 5 simulations with different potential energy functions (i.e., different perturbations). The red line is the time necessary to perform one single simulation and to compute the Girsanov formula on fly for 1, ..., 5 different perturbations at the same time. The benchmark test has been realized on a CPU Intel(R) Core(TM) i5-4590 CPU @ 3.30 GHz with 15 GB of RAM.

B. Stochastic forces

The dynamical reweighting method has been derived by using the Langevin equation of motion as the starting point. It relies on the assumption that the random forces are generated by a Wiener process (Appendix B), and it can hence be used directly for MD simulations thermostatted by a Brownian or a Langevin thermostat.

However from a physical perspective, the Langevin dynamics only approximates the Hamiltonian dynamics of the complete system, by splitting the system in a subsystem S and a heat bath B and replacing the interaction of the subsystem with the heat bath by a friction term and a stochastic process. To develop a dynamical reweighting method for a Hamiltonian dynamics simulation, one could split the system into two subsystems S and B , measure the forces which subsystem B exerts on subsystem S , and use these forces as a substitute for the random forces in the path probability ratio. We have tested this on alanine dipeptide by performing a simulation in explicit solvent. We measured the force distribution of the bath degrees of freedom on the heavy atoms of alanine dipeptide and found that they considerably differ from a Gaussian distribution (Fig. 4). Moreover, we would expect that the random forces do not fulfill the usual goodness-criteria of a random number generator. Thus, overall we are skeptical that estimating a substitute for the random forces from a Hamiltonian dynamics simulation, including simulations thermostatted by the Nosé-Hoover or the Berendsen thermostat, will be successful.

Other thermostats, such as the velocity-rescaling or the Andersen thermostat, use random numbers which are however not converted into a Wiener process. For the time-discrete trajectories generated by MD simulations with these thermostats, it is possible to derive reweighting schemes based on the probability of the sequence of random numbers. However, as explained in Appendixes A and B, the path probability ratio would diverge in the limit of continuous paths.

We therefore decided to use the Langevin leapfrog integrator³⁵ to integrate the Langevin equation of motion for both the implicit and explicit solvent simulations and used the random forces generated by the integrator to reweight the path ensemble.

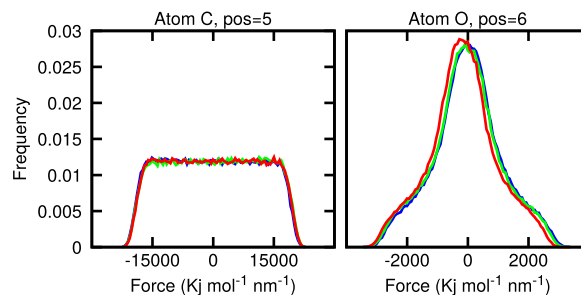


FIG. 4. Distribution of the force of the solvent on the 5th and 6th atoms of the alanine dipeptide. (Blue) Force on the x direction, (green) force on the y direction, and (red) force on the z direction.

C. Two-dimensional system

As a first application, we consider the Brownian dynamics of a particle moving on a two-dimensional potential energy function [Eq. (39)]. The reference potential energy function $V(x, y)$ [Eq. (40), Fig. 5(A)] has two minima at $(-1, -1)$ and $(1, 1)$ which are connected by a transition state at $(0, 0)$. We added a perturbation [Eq. (41)] which tilts the energy function $\tilde{V}(x, y)$ along the direction y , such that the minimum at $(1, 1)$ becomes much deeper than the minimum at $(-1, -1)$. Figures 5(B) and 5(E) show the dominant left MSM eigenvectors of the two systems (direct MSMs). The first eigenvector corresponds to the equilibrium distribution. In both cases, the second eigenvector represents the transition between the two wells, while the third eigenvector corresponds to an exchange of probability density between the transition state region and the two wells.

Figure 5(C) shows the MSM eigenvectors obtained by reweighting the simulation in $V(x, y)$ to the perturbed potential energy function $V(x, y) + U(y)$ (reweighted MSM). Both eigenvectors [Eq. (31)] and implied time scales [Eq. (32)] are in perfect agreement with Fig. 5(E). This confirms that reweighting MSMs using the Girsanov formula works well for a low-dimensional Brownian dynamics.²⁹ Note that the simulation in the reference potential energy function $V(x, y)$ exhibits frequent transitions between the two minima, and thus Eq. (24) is certainly fulfilled. By contrast, in the perturbed system $\tilde{V}(x, y)$, the simulation sampled considerably fewer transitions

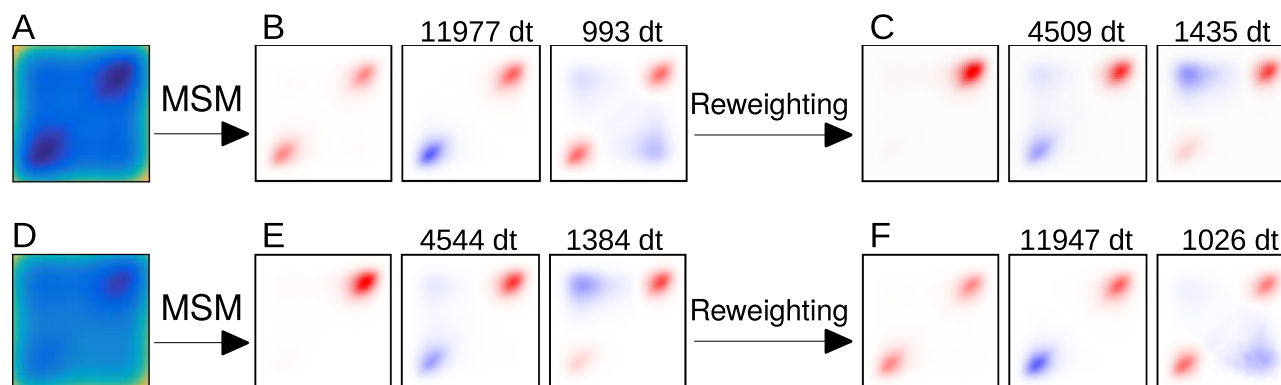


FIG. 5. Two-dimensional system. (A) Reference potential. (B) Dominant left eigenvectors of the reference potential. (C) Dominant left eigenvectors reweighted from the reference dynamics. (D) Perturbed potential. (E) Dominant left eigenvectors of the perturbed potential. (F) Dominant left eigenvectors reweighted from the perturbed dynamics.

between the minima and only a small fraction of the simulation time was spent in the minimum in the lower left corner. Figure 5(F) shows the dominant eigenvectors of a MSM of the reference dynamics constructed by reweighting the perturbed path ensemble. The fact that Fig. 5(C) is in excellent agreement with Fig. 5(B) demonstrates that the reweighting method yields accurate results even for path ensembles with low numbers of transitions across the largest barriers of the system and thus suggests that it can be applied to high-dimensional dynamics on rugged potential energy surfaces.

D. Many-body system in three-dimensional space

As a second example, we studied a six-particle system, in which five particles form a chain while the sixth particle branches the chain at the central atom Fig. 6(a). We constructed the MSM on the central bonds \mathbf{r}_{12} and \mathbf{r}_{13} but applied the

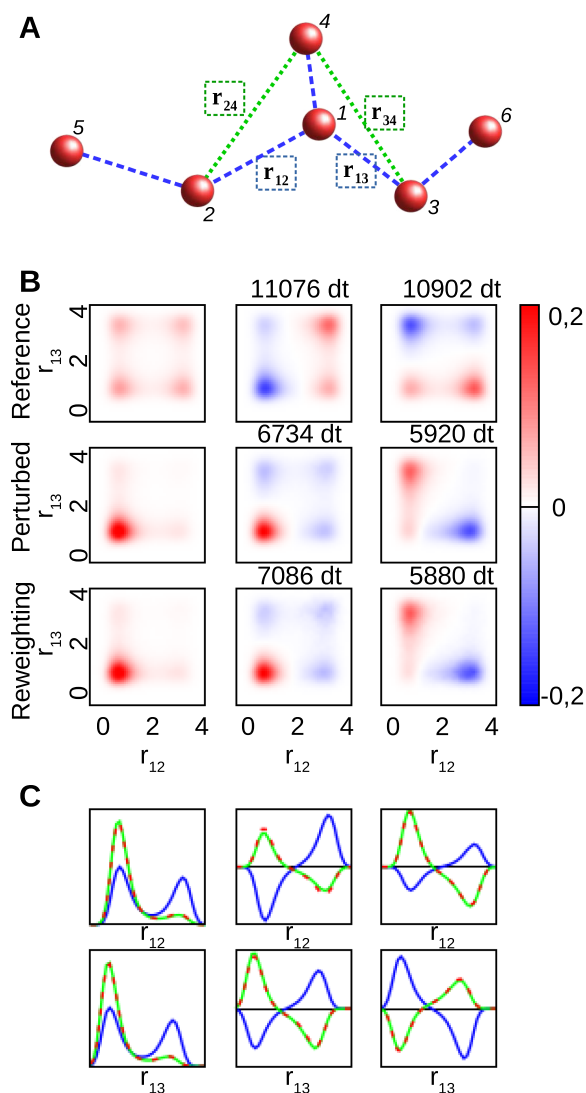


FIG. 6. Many-body system. (a) The perturbation acts on \mathbf{r}_{24} and \mathbf{r}_{34} , while the MSM is constructed on the distances \mathbf{r}_{12} and \mathbf{r}_{13} . (b) Dominant eigenvectors obtained by direct simulations of the reference and perturbed system and by reweighting the reference simulation. (c) Eigenvectors projected on the coordinates \mathbf{r}_{12} and \mathbf{r}_{13} : blue: reference, green: perturbed, and red: reweighted.

perturbation potential energy function along the through-space distances \mathbf{r}_{24} and \mathbf{r}_{34} . Thus, the perturbation was projected onto the reaction coordinates \mathbf{r}_{12} and \mathbf{r}_{13} during the reweighting. The reference potential energy function for each bond is a tilted double well potential, such that the reference system exhibits four metastable states [first row of Fig. 6(b)]. The six-particle system and the reference potential energy function are symmetric. Thus the MSM of the reference system has two degenerate dominant eigenvectors with implied time scales of $1.1 \cdot 10^4 \Delta t$.

The perturbation contracts the bonds, thereby stabilizing the metastable state at the lower left corner in the 1st eigenvector [second row of Fig. 6(b)]. Its effect is to break the symmetry and to accelerate the dynamics, yielding implied time scales of $6.7 \cdot 10^4 \Delta t$ and $5.9 \cdot 10^4 \Delta t$. The third row of Fig. 6(b) shows the eigenvectors and the implied time scales obtained by reweighting the simulation at the reference potential energy function to the perturbed potential energy function. The projection of the eigenvectors [Fig. 6(b)] demonstrates that the direction simulations of the perturbed system and the reweighted model are in almost perfect agreement. The relative error of the implied time scale of the second and third eigenvectors is 5.2% and 0.7%, respectively.

E. Alanine dipeptide and valine dipeptide

Figure 7 shows the results for alanine dipeptide (Ac-A-NHMe) in implicit water. The MSM has been constructed on the ϕ and ψ backbone dihedral angles, and the slow eigenvectors of the unperturbed system are shown in Fig. 7(c). The first eigenvector shows the typical equilibrium distribution in the Ramachandran plane.⁴¹ The second eigenvector represents torsion around the ϕ angle and corresponds to a kinetic exchange between the L_α -minimum ($\phi > 0$) and the α -helix and β -sheet minima ($\phi < 0$). The associated time scale is 2.8 ns. The green arrows in Fig. 7(c) represent the frequency of the transitions, with the transition $L_\alpha \leftrightarrow \beta$ -sheet conformation occurring more frequently than the transition $L_\alpha \leftrightarrow \alpha$ -helical conformation. The third eigenvector represents a transition β -sheet $\leftrightarrow \alpha$ -helical conformation, i.e., torsion around ψ , and is associated with a time scale of 27 ps.

We perturbed the dynamics by adding a harmonic potential to the dihedral angle potentials of the ϕ - and ψ -angle [Figs. 7(a) and 7(b), Eq. (47) with $\kappa_\phi = 0.5$ and $\kappa_\psi = 0.5$]. The α -helical region is somewhat stabilized by the perturbation but otherwise the dominant eigenvectors are very similar to the unperturbed system [second row in Fig. 7(c)]. However, the perturbation changes the relative frequency of the two possible transitions (green arrows) in the second eigenvector, resulting in an increased implied time scale of 4.5 ns. The third row of Fig. 7(c) shows the dominant eigenvectors of the perturbed system obtained by reweighting the reference simulations, and Fig. 7(d) shows the projection of the eigenvectors of all three models onto the ϕ - and ψ -torsion angle. The reweighted model is in excellent agreement with the direct simulation of the perturbed systems. The relative error of the implied time scale associated with the second eigenvector is 4.1%.

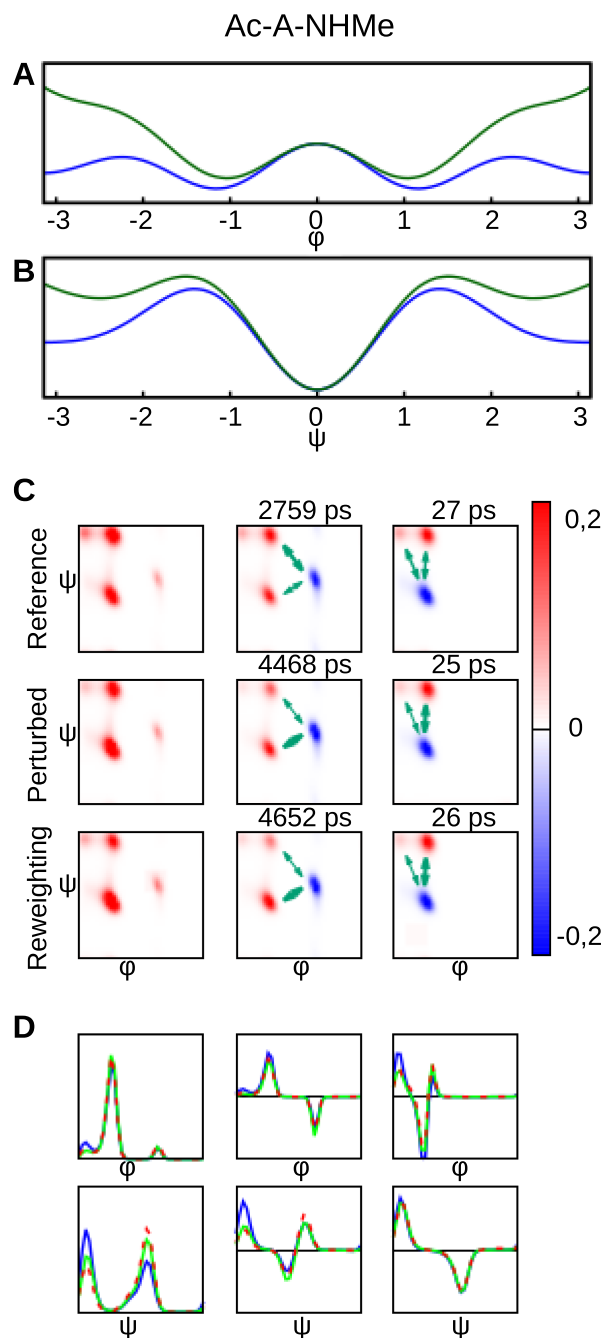


FIG. 7. Alanine dipeptide. (a) Potential energy function along ϕ : blue: reference potential energy function $V(\phi)$ [Eq. (45)], green: perturbed potential energy function $V(\phi) + U(\kappa_\phi = 0.5, \kappa_\psi = 0, \phi, \psi)$ [Eq. (47)]. (b) Potential energy function along ψ : blue: $V(\psi)$ [Eq. (46)], green: $V(\psi) + U(\kappa_\phi = 0, \kappa_\psi = 0.5, \phi, \psi)$ [Eq. (47)]. (c) Dominant MSM eigenvectors of alanine dipeptide. (d) Eigenvalues projected onto the ϕ and ψ backbone torsion angles: blue: reference, green: perturbed, and red: reweighted.

Figure 8(a) shows the implied time scale test [Eq. (32)] for alanine dipeptide in implicit water. All three systems (reference, perturbed, and reweighted) show constant implied time scales, indicating that the MSMs are well converged. Moreover, the graph shows that the reweighting method can recover the implied time scales of the perturbed system over a large range of lag times τ . We have repeated the alanine dipeptide simulations in explicit water. The eigenvectors are very similar to those of alanine dipeptide in implicit water

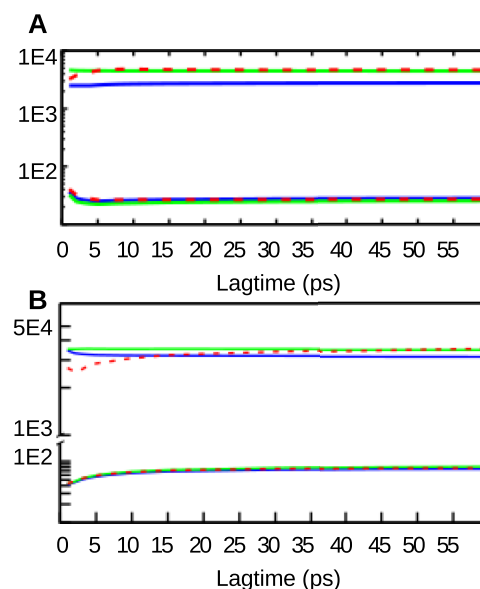


FIG. 8. Alanine dipeptide. (a) Implied time scales in implicit solvent. (b) Implied time scales in explicit solvent. Reference potential (blue line), perturbed potential (green line), and reweighting method (red dashed line).

(data not shown), but the associated implied time scales differ from the implicit solvent simulations [Fig. 8(b)]. In the unperturbed system, the implied time scale of the second eigenvector was 3.1 ns and the implied time scale of the third eigenvector was 75 ps. Perturbing the dihedral angle potentials slightly increased the implied time scale of the second eigenvector to 3.5 ns and left the implied time scale of the third eigenvector unaffected. The implied time scales of the reference simulation and the direct simulation of the perturbed system were constant, whereas we noticed a slight drift in the implied time scale of the second eigenvector for the reweighted MSM. At $\tau = 45$ ps, the measured implied time scale is 3.4 ns which corresponds to a relative error of 2.8%.

We also tested the dynamical reweighting method on valine dipeptide (Fig. 9). Here, however, we perturbed the potential energy function of the χ -side chain dihedral angle [Fig. 9(a)] by adding a harmonic potential, while constructing the MSM on the ϕ and ψ backbone dihedral angles. Thus, the perturbation did not directly act on the variables of the MSM. The perturbation of the χ angle had no effect on the eigenvectors of the MSM [Fig. 9(b)], but it did change the implied time scales. It caused a decrease of the implied time scale of the second eigenvector from 1.3 ns in the reference simulation to 1.0 ns in the perturbed simulation and a slight increase of the implied time scale of the third eigenvector from 159 ps in the reference simulation to 170 ps in the perturbed simulation. Reweighting the reference simulation to the perturbed potential energy function recovered the results of the direct simulation of the perturbed system. The implied time scales obtained by the reweighting calculation were 1.0 ns (relative error: 4.9% before rounding to ns) for the second eigenvector and 179 ps (relative error: 5.3%) for the third eigenvector. This shows that the dynamical reweighting method also works, when the perturbation acts on degrees of freedom which are not part of the relevant coordinates on which the MSM is constructed.

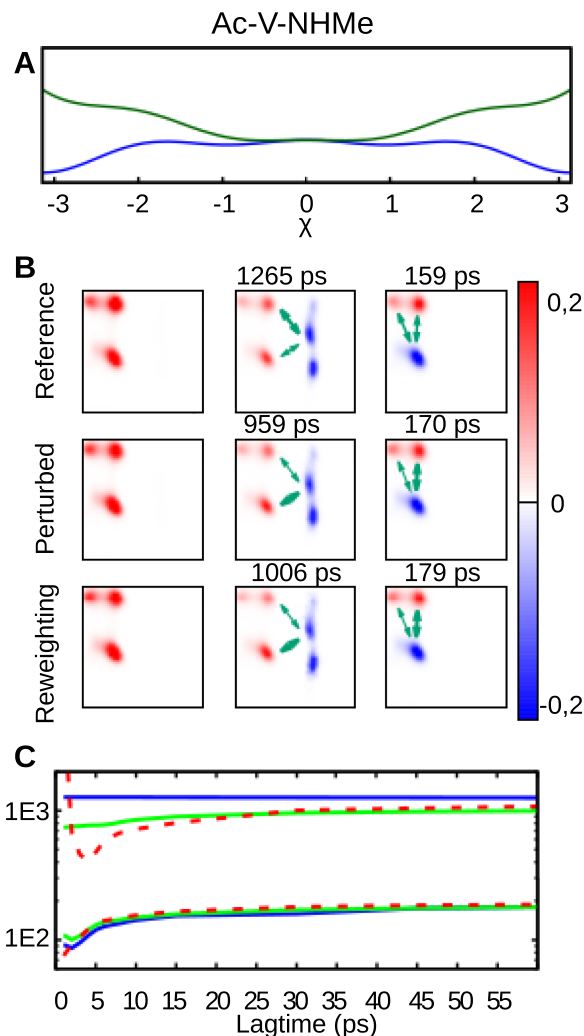


FIG. 9. Valine dipeptide. (a) Reference potential energy function of the side-chain dihedral angle χ , $V(\chi)$ (blue line), and perturbed potential energy function, $V(\chi) + U(\kappa_\chi = 0.5, \chi)$ (green line). (b) First three MSM eigenvectors of the valine dipeptide, where the MSM is constructed in the space spanned by the ϕ - and ψ -backbone dihedral angle. (c) Associated implied time scales as a function of the lag time τ . Reference potential (blue line), perturbed potential (green line), and reweighting method (red dashed line).

Figure 10 illustrates how to use the dynamical reweighting method to study the influence of a force constant on the molecular dynamics. It shows the implied time scale of the second and third MSM eigenvectors of alanine dipeptide in explicit water as a function of the force constant κ_ϕ , where the perturbation potential energy is given by Eqs. (45) and (47). The scan has been repeated with different values of the force constant κ_ψ for the potential energy function of the ψ -backbone dihedral angle [Eqs. (46) and (47)]. The dynamics is more sensitive to a change in the value of κ_ϕ than to a change of κ_ψ , but the overall effect of the perturbation is moderate. It is important to point out that MSMs which are summarized in Fig. 10 have been constructed from a single simulation at the reference potential energy function. During this simulation, the Itô integral $I(a)$ and the Riemann integral $R(a)$ have been calculated for $\kappa_\phi = 1$ and $\kappa_\psi = 1$, and the force constants have been scaled after the simulation during the construction of the MSM, as described in Sec. IV A.

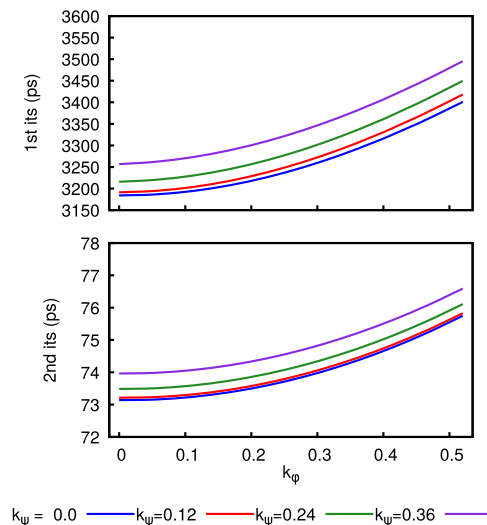


FIG. 10. First and second implied time scales of alanine dipeptide in explicit solvent as a function of the parameters κ_ϕ , κ_ψ , estimated with the Girsanov reweighting methods.

V. CONCLUSION

We have presented the Girsanov reweighting scheme, which is a method to study the dynamics of a molecular system subject to an (external) perturbation $U(\kappa, \mathbf{x})$ of the (reference) potential energy function $V(\mathbf{x})$. It allows for the estimation of a dynamical model, e.g., a MSM, of the perturbed system from a simulation at the reference potential energy function. The underlying assumption is that the equation of motion generates a path ensemble and that we can define a probability measure on this ensemble. A perturbation of the potential energy function causes modification of the probability measure. The Girsanov theorem guarantees that the probability ratio between these two measures exists (under certain conditions) and leads to an analytical expression for this ratio [Eq. (25)]. By reformulating the MSM transition probabilities as path ensemble averages, we can apply the Girsanov reweighting scheme to obtain the transition probabilities of the perturbed system from a set of paths generated at the reference potential energy function. The method can be extended to the variational approaches,^{42,43} milestone approaches,^{44,45} or tensor approaches⁴⁶ to molecular dynamics, since in each of these methods the molecular transfer operator is discretized and the resulting matrix elements are estimated as path ensemble averages.

Calculating the path probability ratio requires knowledge of the random forces at each integration time step. For the explicit solvent simulations, we have introduced stochastic forces by using a Langevin thermostat. In an efficient implementation of the method, two terms which are needed to calculate the probability ratio should be calculated “on the fly” during the simulation. We have demonstrated this using the MD simulation toolkit OPENMM.³²

Two other dynamical reweighting schemes for MSMs have been published in recent years. In the reweighting scheme for parallel tempering simulations,^{47,48} the path probability density is defined for time discretized paths at a reference temperature and then reweighted to different temperatures

using statistically optimal estimators.^{49,50} Like the Girsanov reweighting scheme, this method relies on the random forces at each integration time step and reweights the contribution of each path to the estimate of the transition probability individually. We remark that the reweighting to different thermodynamic states cannot be extended to the limiting case of continuous paths because for different volatilities the path probability ratio relative to the Wiener process cannot be defined (see Appendix A). This however seems to be of little practical importance. In the Transition-Based Reweighting Analysis Method (TRAM),^{51–53} rather than reweighting the probabilities of each individual path, the MSM transition probabilities $T_{ij}(\tau)$ are directly reweighted to a different potential energy function or a different thermodynamic state using a maximum likelihood estimator for the transition counts. This becomes possible, if one additionally assumes that the dynamics is in local equilibrium within each microstate of the MSM, which possibly renders the method more sensitive to the MSM discretization than path-based reweighting methods.

We have tested the Girsanov reweighting method on several systems, ranging from diffusion in a two-dimensional potential energy surface to alanine dipeptide and valine dipeptide in implicit and explicit water. Importantly, the direct simulations of the perturbed potential energy function (Figs. 6, 7, and 9) are only included as a validation for the method. In an actual application, one would only simulate the system at the reference potential energy function and then reweight to the perturbed potential energy function, thus saving the computational time of the direct simulation of the perturbed system.

Girsanov reweighting could be useful in several areas of research. First, one can very efficiently test the influence of a change in the potential energy function on the dynamics of the molecule. The influence of a change in the force constant on the dynamics is particularly easy to study. The Girsanov reweighting method can therefore be applied to improve the dynamical properties of force fields,⁴¹ by, for example, tuning the force constants to match an experimentally measured correlation time. Similarly, one can use Girsanov reweighting to understand the influence of restraining potentials^{54,55} on the dynamics of the system. Second, the method can be used to understand which degrees of freedom have the largest influence on the slow modes of the molecule.^{56,57} For example, for alanine dipeptide, we showed that the slow dynamic modes are more sensitive to a force field variation in the ϕ -backbone dihedral angle than they are to a variation in the ψ -backbone dihedral angle. Last but not least, Girsanov reweighting can be used to account for the effect of any external potential which has been added to the simulation in order to enhance the sampling. Thus, one can, for example, estimate MSMs from metadynamics simulations,^{58,59} Hamilton replica exchange simulations,⁶⁰ or umbrella sampling simulations.⁶¹

SUPPLEMENTARY MATERIAL

See [supplementary material](#) for the example script for the implementation of the dynamical reweighting method with OpenMM.³²

ACKNOWLEDGMENTS

This research has been funded by Deutsche Forschungsgemeinschaft (DFG) through Grant No. CRC 1114 “Scaling Cascades in Complex Systems,” Project A05 “Probing scales in equilibrated systems by optimal nonequilibrium forcing,” and Project B05 “Origin of the scaling cascades in protein dynamics.”

APPENDIX A: TIME-DISCRETE AND CONTINUOUS PATH SPACE MEASURES

Path probability densities of time-discrete paths are derivatives with respect to the Lebesgue measure $d\omega = dx_1 dx_2 \dots dx_n$, i.e., $\mu_P(\omega) = dP/d\omega$. Here, we discuss why it is difficult to extend the concept of path probability densities to time-continuous paths. Consider a diffusion process $x_t \in \Gamma \subset \mathbb{R}$ which is a solution of the stochastic differential equation

$$dx_t = a(x_t)dt + \sigma dB_t, \quad 0 \leq t \leq \tau, \quad (\text{A1})$$

where $a(\cdot)$ is a drift, B_t is a Brownian motion, σ is a volatility, and τ is the total time. Discretizing Eq. (A1) using the Euler-Maruyama method yields⁶²

$$x_{k+1} = x_k + a_k \Delta t + \eta_k \sigma \sqrt{\Delta t}, \quad 0 \leq k \leq n, \quad (\text{A2})$$

where $a_k = a(x_k)$, Δt is a time step, and η_k is a random number drawn from a standard Gaussian distribution. Iterating Eq. (A2) n times generates a *time-discrete path* as defined in Sec. II B. Likewise, the path space is $\Omega_{\tau,x} = \Gamma^n$. The path probability measure P and the associated path probability density $\mu_P(\omega)$ are given by Eqs. (6) and (7), respectively.

For a Brownian motion with drift, there is an analytical expression for the transition probability density $p(x_k, x_{k+1}; \Delta t)$ of time-discrete paths,

$$p(x_k, x_{k+1}; \Delta t) = \frac{1}{\sqrt{2\pi\Delta t\sigma^2}} \exp\left(-\frac{(x_{k+1} - x_k - a_k \Delta t)^2}{2\Delta t\sigma^2}\right). \quad (\text{A3})$$

The probability density of a path (x_0, x_1, \dots, x_n) conditional on starting at x_0 is then simply given by the product of the corresponding transition probabilities,

$$\begin{aligned} \mu_P(x_1, \dots, x_n; x_0) &= \left(\frac{1}{\sqrt{2\pi\Delta t\sigma^2}}\right)^n \\ &\times \exp\left(-\frac{\Delta t}{2\sigma^2} \sum_{k=1}^n \left(\frac{x_{k+1} - x_k}{\Delta t} - a_k\right)^2\right). \end{aligned} \quad (\text{A4})$$

Ideally, one would like to see the continuous path density on the space of, say, continuous curves, to emerge in the limit $\Delta t \rightarrow 0$, $n \rightarrow \infty$ with $n\Delta t \rightarrow \tau$. However, a short moment of reflection convinces us that this cannot be the case: First, the normalization constant, the denominator in (A4), diverges as $\Delta t \rightarrow 0$ and $n \rightarrow \infty$. Second, the paths of the Brownian motion are nowhere differentiable and, as a consequence, the term $(x_{k+1} - x_k)/\Delta t$ in the path density becomes ill-defined. Third, the reference measure in $\mu_P = dP/d\omega$ is the n -dimensional Lebesgue measure $d\omega$ that has no meaning for $n \rightarrow \infty$.

APPENDIX B: DERIVATION OF THE GIRSANOV FORMULA

We now show how the problems described in [Appendix A](#) can be solved by considering path densities with respect to reference measure other than the Lebesgue measure, which then gives rise to the Girsanov formula. We note that our short derivation stays purely formal and is given for the reader's convenience. The interested reader may consult standard textbooks on Stochastic Differential Equations (SDEs).^{28,63} Analogously to Eqs. (A1) and (A2), we define a second diffusion process with initial conditions $x_0 = x \in \mathbb{R}$ by

$$dx_t = b(x_t) dt + \sigma dB_t \quad (\text{B1})$$

and

$$x_{k+1} = x_k + b_k \Delta t + \eta_k \sigma \sqrt{\Delta t}. \quad (\text{B2})$$

Given a particular path ω starting at x_0 , the likelihood ratio of the corresponding transition probability densities is given by

$$M_{\tau,x}(\omega) = \frac{\mu_{P_b}(\omega)}{\mu_{P_a}(\omega)} = \frac{\prod_{k=1}^n \exp\left(-\frac{(x_{k+1}-x_k-b_k\Delta t)^2}{2\Delta t\sigma^2}\right)}{\prod_{k=1}^n \exp\left(-\frac{(x_{k+1}-x_k-a_k\Delta t)^2}{2\Delta t\sigma^2}\right)}. \quad (\text{B3})$$

In Eq. (B3), the normalization constants get canceled which solves the first problem mentioned in [Appendix A](#). Rearranging the fraction, moving the product into the exponent, and expanding the quadratic terms yield

$$\begin{aligned} M_{\tau,x}(\omega) &= \exp\left(\sum_{k=0}^n \frac{-(x_{k+1}-x_k-b_k\Delta t)^2 + (x_{k+1}-x_k-a_k\Delta t)^2}{2\Delta t\sigma^2}\right) \\ &= \exp\left(\sum_{k=0}^n \frac{(b_k^2 - a_k^2)\Delta t^2 - 2x_{k+1}(b_k - a_k)\Delta t + 2x_k(b_k - a_k)\Delta t}{2\Delta t\sigma^2}\right) \\ &= \exp\left(\sum_{k=0}^n \frac{(x_{k+1}-x_k)(b_k - a_k)}{\sigma^2}\right) \exp\left(-\sum_{k=0}^n \frac{(b_k^2 - a_k^2)\Delta t}{2\sigma^2}\right). \end{aligned} \quad (\text{B4})$$

In the second line, terms which do not contain either $a_k\Delta t$ or $b_k\Delta t$ cancel. Hence, Δt cancels in the overall expression and hence the time derivative of x_t does not appear. This solves the second problem from [Appendix A](#).

The remaining terms have straightforward interpretations: Taking the limit $\Delta t \rightarrow 0$ and $n \rightarrow \infty$ such that $n\Delta t \rightarrow \tau$, the exponent in the second term of (B4) converges to a Riemann integral,

$$\lim_{\Delta t \rightarrow 0} \sum_{k=0}^n \frac{(b_k^2 - a_k^2)\Delta t}{2\sigma^2} = \frac{1}{2} \int_0^\tau \frac{b(x_s)^2 - a(x_s)^2}{\sigma^2} ds. \quad (\text{B5})$$

The first term converges to an Itô integral, at least formally. More specifically, using (A1),

$$\lim_{\Delta t \rightarrow 0} \sum_{k=0}^n (b_k - a_k)(x_{k+1} - x_k) = \int_0^\tau (b(x_s) - a(x_s)) dx_s = \int_0^\tau (b(x_s) - a(x_s)) (a(x_s) ds + \sigma dB_s). \quad (\text{B6})$$

Inserting (B5) and (B6) into Eq. (B4) yields the Girsanov formula

$$\begin{aligned} \lim_{\Delta t \rightarrow 0} M_{\tau,x}(\omega) &= \exp\left(\int_0^\tau \frac{a(x_s)b(x_s)ds + b(x_s)\sigma dB_s - a(x_s)^2 ds - a(x_s)\sigma dB_s}{\sigma^2}\right) \exp\left(-\frac{1}{2} \int_0^\tau \frac{b(x_s)^2 - a(x_s)^2}{\sigma^2} ds\right) \\ &= \exp\left(\int_0^\tau \frac{b(x_s)\sigma dB_s - a(x_s)\sigma dB_s}{\sigma^2}\right) \exp\left(\int_0^\tau \frac{a(x_s)b(x_s) - a(x_s)^2}{\sigma^2} ds - \frac{1}{2} \int_0^\tau \frac{b(x_s)^2 - a(x_s)^2}{\sigma^2} ds\right) \\ &= \exp\left(\int_0^\tau \frac{b(x_s) - a(x_s)}{\sigma} dB_s\right) \exp\left(-\frac{1}{2} \int_0^\tau \frac{(b(x_s) - a(x_s))^2}{\sigma^2} ds\right). \end{aligned} \quad (\text{B7})$$

Equation (B7) is an analytical expression for the likelihood ratio of time-continuous paths. In other words, even though the probability densities of the discrete paths have no straightforward extension to the continuous case, their likelihood ratio is always well defined, provided that the two processes are driven by the same Gaussian noise process to yield cancellation of the problematic terms (and further technical integrability conditions).

In this paper, we use the Euler-Maruyama discretization

$$\begin{aligned} M_{\tau,x}(\omega) &= \exp\left(\sum_{k=0}^n \frac{(b_k - a_k)\eta_k \sqrt{\Delta t}}{\sigma}\right) \\ &\quad \times \exp\left(-\frac{1}{2} \sum_{k=0}^n \frac{(b_k - a_k)^2 \Delta t}{\sigma^2}\right) \end{aligned} \quad (\text{B8})$$

of the Girsanov formula (B7) which is consistent with the Euler-Maruyama discretization of the corresponding SDEs.

- ¹P. G. Bolhuis, D. Chandler, C. Dellago, and P. L. Geissler, *Annu. Rev. Phys. Chem.* **53**, 291 (2002).
- ²A. K. Faradjian and R. Elber, *J. Chem. Phys.* **120**, 10880 (2004).
- ³R. B. Best and G. Hummer, *Proc. Natl. Acad. Sci. U. S. A.* **102**, 6732 (2005).
- ⁴R. Hegger and G. Stock, *J. Chem. Phys.* **130**, 034106 (2009).
- ⁵P. Faccioli, A. Lonardi, and H. Orland, *J. Chem. Phys.* **133**, 045104 (2010).
- ⁶C. Schütte, A. Fischer, W. Huisinga, and P. Deuffhard, *J. Comput. Phys.* **151**, 146 (1999).
- ⁷C. Schütte, W. Huisinga, and P. Deuffhard, in *Ergodic Theory, Analysis, and Efficient Simulation of Dynamical Systems*, edited by B. Fiedler (Springer, 2001), pp. 191–223.
- ⁸P. Deuffhard, W. Huisinga, A. Fischer, and C. Schütte, *Linear Algebra Appl.* **315**, 39 (2000).
- ⁹W. C. Swope, J. W. Pitera, F. Suits, M. Pitman, M. Eleftheriou, B. G. Fitch, R. S. Germain, A. Rayshubski, T. J. C. Ward, Y. Zhestkov, and R. Zhou, *J. Phys. Chem. B* **108**, 6582 (2004).
- ¹⁰J. D. Chodera, N. Singhal, V. S. Pande, K. A. Dill, and W. C. Swope, *J. Chem. Phys.* **126**, 155101 (2007).
- ¹¹N.-V. Buchete and G. Hummer, *J. Phys. Chem. B* **112**, 6057 (2008).
- ¹²J.-H. Prinz, H. Wu, M. Sarich, B. G. Keller, M. Senne, M. Held, J. D. Chodera, C. Schütte, and F. Noé, *J. Chem. Phys.* **134**, 174105 (2011).
- ¹³B. G. Keller, X. Daura, and W. F. Van Gunsteren, *J. Chem. Phys.* **132**, 074110 (2010).
- ¹⁴B. G. Keller, P. Hünenberger, and W. F. van Gunsteren, *J. Chem. Theory Comput.* **7**, 1032 (2011).
- ¹⁵V. A. Voelz, G. R. Bowman, K. A. Beauchamp, and V. S. Pande, *J. Am. Chem. Soc.* **132**, 1526 (2010).
- ¹⁶N. Stanley, S. Esteban-Martin, and G. D. Fabritiis, *Nat. Commun.* **5**, 5272 (2014).
- ¹⁷G. R. Bowman, E. R. Bolin, K. M. Hart, B. C. Maguire, and S. Marqusee, *Proc. Natl. Acad. Sci. U. S. A.* **112**, 2734 (2015).
- ¹⁸N. Plattner and F. Noé, *Nat. Commun.* **6**, 7653 (2015).
- ¹⁹L. Zhang, F. Pardo-Avila, I. C. Unarta, P. P.-H. Cheung, G. Wang, D. Wang, and X. Huang, *Acc. Chem. Res.* **49**, 687 (2016).
- ²⁰R. Zwanzig, *J. Chem. Phys.* **22**, 1420 (1954).
- ²¹C. H. Bennett, *J. Comput. Phys.* **22**, 245 (1976).
- ²²S. Kumar, D. Bouzida, R. H. Swendsen, P. A. Kollman, and J. M. Rosenberg, *J. Comput. Chem.* **13**, 1011 (1992).
- ²³J. Kästner and W. Thiel, *J. Chem. Phys.* **123**, 144104 (2005).
- ²⁴B. Lapeyre, E. Pardoux, and R. Sentis, *Méthodes de Monte Carlo pour les équations de transport et de diffusion* (Springer, Berlin, 1998).
- ²⁵O. Papaspiliopoulos and G. Roberts, University of Warwick, Centre for Research in Statistical Methodology, Working Papers, No. 28, 2009.
- ²⁶C. Hartmann and C. Schütte, *J. Stat. Mech.: Theory Exp.* **2012**, P11004.
- ²⁷I. V. Girsanov, *Theory Probab. Its Appl.* **5**, 285 (1960).
- ²⁸B. Øksendal, *Stochastic Differential Equations: An Introduction with Applications*, 6th ed. (Springer Verlag, Berlin, 2003), pp. 139–167.
- ²⁹C. Schütte, A. Nielsen, and M. Weber, *Mol. Phys.* **113**, 69 (2015).
- ³⁰E. Platen and N. Bruti-Liberati, *Numerical Solution of Stochastic Differential Equations with Jumps in Finance* (Springer Verlag, Berlin, 2010), p. 246.
- ³¹A. Brünger, C. L. Brooks III, and M. Karplus, *Chem. Phys. Lett.* **105**, 495 (1984).
- ³²P. Eastman, M. S. Friedrichs, J. D. Chodera, R. J. Radmer, C. M. Bruns, J. P. Ku, K. A. Beauchamp, T. J. Lane, L.-P. Wang, D. Shukla, T. Tye, M. Houston, T. Stich, C. Klein, M. R. Shirts, and V. S. Pande, *J. Chem. Theory Comput.* **9**, 461 (2013).
- ³³J. A. Maier, C. Martinez, K. Kasavajhala, L. Wickstrom, K. E. Hauser, and C. Simmerling, *J. Chem. Theory Comput.* **11**(8), 3696 (2015).
- ³⁴A. Onufriev, D. Bashford, and D. A. Case, *Proteins* **55**, 383 (2004).
- ³⁵J. A. Izaguirre, C. R. Sweet, and V. S. Pande, “Multiscale dynamics of macromolecules using normal mode Langevin,” in *Pacific Symposium on Biocomputing 2010* (World Scientific, 2010), pp. 240–251.
- ³⁶U. Essmann, L. Perera, M. L. Berkowitz, T. Darden, H. Lee, and L. G. Pedersen, *J. Chem. Phys.* **103**, 8577 (1995).
- ³⁷D. Van Der Spoel, E. Lindahl, B. Hess, G. Groenhof, A. E. Mark, and H. J. Berendsen, *J. Comput. Chem.* **26**, 1701 (2005).
- ³⁸K. Lindorff-Larsen, S. Piana, K. Palmo, P. Maragakis, J. Klepeis, R. Dror, and D. E. Shaw, *Proteins* **78**, 1950 (2010).
- ³⁹W. L. Jorgensen, J. Chandrasekhar, J. D. Madura, R. W. Impey, and M. Klein, *J. Chem. Phys.* **79**, 926 (1983).
- ⁴⁰G. Bussi, D. Donadio, and M. Parrinello, *J. Chem. Phys.* **126**, 014101 (2007).
- ⁴¹F. Vitalini, A. S. J. S. Mey, F. Noé, and B. G. Keller, *J. Chem. Phys.* **142**, 084101 (2015).
- ⁴²F. Nüske, B. G. Keller, G. Pérez-Hernández, A. S. J. S. Mey, and F. Noé, *J. Chem. Theory Comput.* **10**, 1739 (2014).
- ⁴³F. Vitalini, F. Noé, and B. G. Keller, *J. Chem. Theory Comput.* **11**, 3992 (2015).
- ⁴⁴C. Schütte, F. Noé, J. Lu, M. Sarich, and E. Vanden-Eijnden, *J. Chem. Phys.* **134**, 204105 (2011).
- ⁴⁵O. Lemke and B. G. Keller, *J. Chem. Phys.* **145**, 164104 (2016).
- ⁴⁶F. Nüske, R. Schneider, F. Vitalini, and F. Noé, *J. Chem. Phys.* **144**, 054105 (2016).
- ⁴⁷J.-H. Prinz, J. D. Chodera, V. S. Pande, W. C. Swope, J. C. Smith, and F. Noé, *J. Chem. Phys.* **134**, 244108 (2011).
- ⁴⁸J. D. Chodera, W. C. Swope, F. Noé, J.-H. Prinz, M. R. Shirts, and V. S. Pande, *J. Chem. Phys.* **134**, 244107 (2011).
- ⁴⁹M. R. Shirts and J. D. Chodera, *J. Chem. Phys.* **129**, 124105 (2008).
- ⁵⁰D. D. L. Minh and J. D. Chodera, *J. Chem. Phys.* **131**, 134110 (2009).
- ⁵¹A. S. J. S. Mey, H. Wu, and F. Noé, *Phys. Rev. X* **4**, 041018 (2014).
- ⁵²H. Wu, A. S. J. S. Mey, E. Rosta, and F. Noé, *J. Chem. Phys.* **141**, 214106 (2014).
- ⁵³H. Wu, F. Paul, C. Wehmeyer, and F. Noé, *Proc. Natl. Acad. Sci. U. S. A.* **113**, E3221 (2016).
- ⁵⁴A. Cesari, A. Gil-Ley, and G. Bussi, *J. Chem. Theory Comput.* **12**, 6192 (2016).
- ⁵⁵B. G. Keller, M. Christen, C. Oostenbrink, and W. F. van Gunsteren, *J. Biomol. NMR* **37**, 1 (2007).
- ⁵⁶A. Tsourtis, Y. Pantazis, M. A. Katsoulakis, and V. Harmandaris, *J. Chem. Phys.* **143**, 014116 (2015).
- ⁵⁷G. Arampatzis, M. A. Katsoulakis, and L. Rey-Bellet, *J. Chem. Phys.* **144**, 104107 (2016).
- ⁵⁸T. Huber, A. E. Torda, and W. F. van Gunsteren, *J. Comput.-Aided Mol. Des.* **8**, 695 (1994).
- ⁵⁹A. Laio and M. Parrinello, *Proc. Natl. Acad. Sci. U. S. A.* **99**, 12562 (2002).
- ⁶⁰Y. Sugita and Y. Okamoto, *Chem. Phys. Lett.* **329**, 261 (2000).
- ⁶¹G. Torrie and J. Valleau, *J. Comput. Phys.* **23**, 187 (1977).
- ⁶²P. E. Kloeden and E. Platen, *Numerical Solution of Stochastic Differential Equations* (Springer Verlag, Berlin, 1992).
- ⁶³L. C. G. Rogers and D. Williams, *Diffusions, Markov Processes and Martingales* (Cambridge University Press, Cambridge, 2000).